

AD-A181 012

MRC Technical Summary Report #2968

MODELING OF SHOCKLESS ACCELERATION
OF THIN PLATES USING A TRACKED
RANDOM CHOICE METHOD

Bradley J. Plohr

Mathematics Research Center
University of Wisconsin—Madison
610 Walnut Street
Madison, Wisconsin 53705

February 1987

(Received February 9, 1987)

DTIC
SELECTED
JUN 02 1987
S D D

Approved for public release
Distribution unlimited

Sponsored by

U. S. Army Research Office
P. O. Box 12211
Research Triangle Park
North Carolina 27709

National Science Foundation
Washington, DC 20550

87 5 18 175

UNIVERSITY OF WISCONSIN-MADISON
MATHEMATICS RESEARCH CENTER

MODELING OF SHOCKLESS ACCELERATION OF THIN PLATES USING A
TRACKED RANDOM CHOICE METHOD

Bradley J. Plohr*

Technical Summary Report #2968
February 1987

ABSTRACT

A method for accelerating thin metallic plates to hypervelocities has been proposed by G. McCall.¹⁰ In this method a shock in a propellant generates a strong expansion wave that smoothly accelerates the plate.

We have studied the hydrodynamics of this process in one dimension, both analytically and computationally. The metal was modeled as a stiffened gas, and the corresponding Riemann problem was solved. The asymptotic behavior of the solution was determined analytically. The one-dimensional random choice method, modified so that material boundaries are tracked and the spatial mesh is refined locally, was used to compute the flow; comparison with the asymptotic solution demonstrated its accuracy. With this method, shocks that form within the accelerating plate were accurately resolved, so that possible structural damage to the plate could be evaluated.

AMS (MOS) Subject Classifications: 76-04, 76N10, 76L05, 73D05, 65M25, 65C20,
35L65, 35L67

Key Words: shockless acceleration, Riemann problem, random choice,
front tracking

Work Unit Number 2 (Physical Mathematics)



Availability Codes	
Dist	Avail and/or special
A-1	

*Theoretical Division, Los Alamos National Laboratory, Los Alamos, NM 87545.
Permanent Address: Computer Sciences Department, University of Wisconsin-Madison, Madison, WI 53706.

Sponsored by the U. S. Department of Energy, the United States Army under Contract No. DAAG29-80-C-0041, and the National Science Foundation under Grant DMS-8601766.

MODELING OF SHOCKLESS ACCELERATION OF THIN PLATES USING A
TRACKED RANDOM CHOICE METHOD

Bradley J. Plohr *

Introduction

G. McCall has proposed a method for accelerating a thin metal plate to exceedingly high velocities within a short distance.¹⁰ These hypervelocities, on the order of $1 \text{ cm}/\mu\text{s}$, are difficult to achieve without destroying the plate since the kinetic energy of the plate exceeds its vaporization energy. The acceleration must be rapid enough to attain high velocities within a short distance, on the order of 10 cm, but it must be sufficiently smooth that strong shock waves do not form inside the metal. Furthermore, the compression of the plate resulting from the acceleration must be relieved gradually so that the plate does not spall.

A schematic diagram of the experimental configuration proposed by McCall is shown in Fig. 1. A tube containing a tungsten plate is partially filled with a plastic foam (CH) that serves as a propellant; a low pressure cavity separates the foam from the plate. The energy needed to accelerate the plate is supplied by a planar shock passing through the foam and compressing it. When the shock reaches the end of the foam, the foam expands isentropically into the cavity. At the leading edge of this rarefaction wave is low density, high velocity material, which is followed by material with gradually increasing density and decreasing velocity. As successively denser portions of the foam reach the plate, the pressure behind the plate rises, thereby gradually accelerating the plate. Thus the low pressure cavity intervening between the foam driver and the plate converts the shock wave in the foam into a strong rarefaction wave that smooths the acceleration. Of course, the rising pressure behind the plate produces compression waves in the plate that in general steepen into shock waves. McCall has estimated the formation time for such shock waves and has concluded that shockless acceleration of sufficiently thin plates can be achieved using his method.

A more complete modeling of this hydrodynamic process entails computer simulation. Numerical methods for solving the Euler equations encounter three major difficulties in modeling this flow. First, the mass density varies over a vast range, from the high density in the tungsten plate and the compressed foam to the near-vacuum conditions inside the cavity. Therefore Lagrangian coordinates, which place few mesh blocks in regions of low

* Theoretical Division, Los Alamos National Laboratory, Los Alamos, NM 87545.
Permanent Address: Computer Sciences Department, University of Wisconsin-
Madison, Madison, WI 53706.

Sponsored by the U. S. Department of Energy, the United States Army under
Contract No. DAAG29-86-C-0041, and the National Science Foundation under Grant
DMS-8601766.

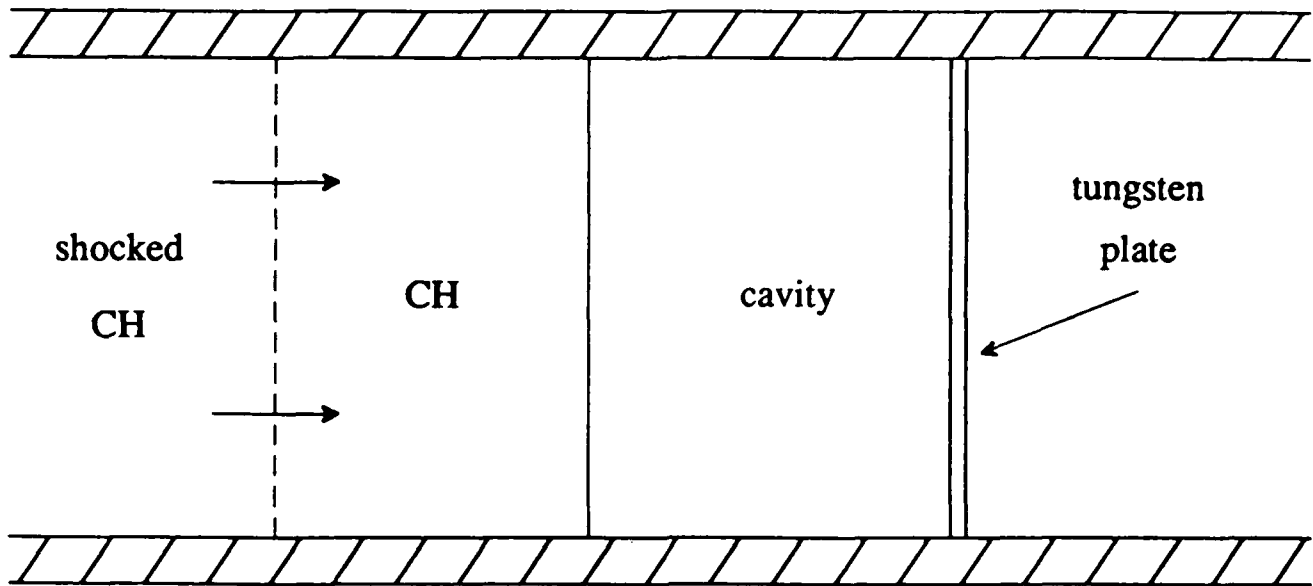


Figure 1. Schematic diagram of the shockless acceleration of a tungsten plate using a plastic foam (CH) propellant. A planar shock in the foam is incident from the left. When it reaches the end of the foam, the foam expands into the cavity. The rarefied foam serves to smoothly accelerate the tungsten.

density, are inappropriate for the leading edge of the rarefaction wave. On the other hand, the material boundary between the metal and the fluid accelerating it is the focus of interest. Whereas the position of this boundary is naturally tracked in Lagrangian coordinates, it is uncertain to within a mesh length on an Eulerian grid; furthermore, most Eulerian methods exhibit substantial numerical diffusion that spreads the interface over many mesh lengths. Finally, the formation of shock waves within the plate must be accurately detected, even though the metal plate is very thin, spanning only a few computational mesh zones.

In this paper we have modeled the hydrodynamics of McCall's problem using a combination of methods that address these difficulties. The computation is performed in Eulerian coordinates to allow for arbitrarily low densities in the cavity. To correctly model the material interfaces, their positions are tracked across the Eulerian grid. Also, the computational mesh is refined in the vicinity of the plate to better resolve the flow in this region. Finally, the underlying numerical scheme for solving the flow equations, the random choice method, models shock waves as sharp discontinuities resolved within a mesh block, so that shock formation can be detected within the thin plate. This numerical approach gives solutions of a much higher quality than were previously available.

The plan of the paper is as follows. In the next section the thermodynamic model we use for the tungsten plate is described. Then the solution of the Riemann problem, which is the key input into the random choice method, is described for this thermodynamic model. Next the random choice method, as extended by front tracking and mesh refinement, is explained. Analytical results on the short-time behavior of flows in which rarefaction waves impinge on a plate are derived in the following section. Finally, the results of numerical experiments for McCall's problem are presented.

Thermodynamics

The shockless acceleration of metal plates will be modeled as a hydrodynamic process. This requires the specification of a suitable equation of state for each component substance. Since use of the random choice method requires that Riemann problems be solved, it is advantageous to use an equation of state that is amenable to analytic solution. The propellant may be modeled as a polytropic gas, for which the solution of the Riemann problem is simple, but the metal plate cannot be adequately modeled as such. In lieu of designing a Riemann solver for a general equation of state, such as one based on the SESAME tables,² we have modeled the metal plate as a "stiffened gas." This equation of state gives the correct semi-quantitative behavior of the plate. In conjunction with a spall model to give yield strains and an estimate of melting and boiling points, it can be used to assess the feasibility of shockless acceleration.

The equation of state for a stiffened gas⁸ is given by the relation

$$E = \frac{1}{\gamma - 1} \frac{p + \gamma p_{\infty}}{\rho}$$

between the specific (internal) energy E , the pressure p , and the mass density ρ . Here γ and p_{∞} are prescribed constants that characterize the gas, γ being dimensionless and p_{∞} being a pressure. In terms of the Grüneisen coefficient

$$\Gamma = \frac{1}{\rho} \left(\frac{\partial p}{\partial E} \right)_{\rho}$$

we have $\gamma = \Gamma + 1$. (Note, however, that γ is not the adiabatic exponent γ_S , which is defined by $c^2 = \gamma_S p / \rho$; see (2.2) below.)

The isentropes for a stiffened gas may be determined by noting that

$$dE + p d\left(\frac{1}{\rho}\right) = \frac{p + p_{\infty}}{\rho} \cdot \frac{1}{\gamma - 1} d \log \left(\frac{p + p_{\infty}}{\rho^{\gamma}} \right). \quad (2.1)$$

Thus the entropy S is most generally given by

$$S = \frac{1}{\gamma - 1} \Sigma \left(\log \left(\frac{p + p_{\infty}}{\rho^{\gamma}} \right) \right)$$

for some function Σ , with the corresponding temperature T being

$$T = \frac{p + p_{\infty}}{\rho} / \Sigma' \left(\log \left(\frac{p + p_{\infty}}{\rho^{\gamma}} \right) \right).$$

The speed of sound c , defined by

$$c^2 = \left(\frac{\partial p}{\partial \rho} \right)_{E} + \frac{p}{\rho^2} \left(\frac{\partial p}{\partial E} \right)_{\rho},$$

may be calculated to be

$$c = \left(\gamma \frac{p + p_{\infty}}{\rho} \right)^{1/2}. \quad (2.2)$$

Fast and slow rarefaction waves, which correspond to the fast and slow characteristic speeds $v \pm c$, satisfy the equations

$$dv \mp \frac{dp}{\rho c} = 0$$

and

$$dE + p d\left(\frac{1}{\rho}\right) = 0.$$

By (2.1) and (2.2) we determine that

$$\frac{dp}{\rho c} = \frac{2}{\gamma - 1} dc.$$

Therefore

$$v \mp \frac{2}{\gamma - 1} c = \text{const.} \quad (2.3)$$

and

$$(p + p_{\infty})/\rho^{\gamma} = \text{const.} \quad (2.4)$$

across rarefactions corresponding to the characteristic speeds

$$v \pm c. \quad (2.5)$$

The Hugoniot locus is given by solving the equation

$$E - E_0 + \frac{1}{2}(p + p_0) \left(\frac{1}{\rho} - \frac{1}{\rho_0} \right) = 0$$

for ρ in terms of ρ_0 , p_0 , and p . Simple algebra yields the result

$$\frac{\rho}{\rho_0} = \frac{(\gamma + 1)(p + p_{\infty}) + (\gamma - 1)(p_0 + p_{\infty})}{(\gamma + 1)(p_0 + p_{\infty}) + (\gamma - 1)(p + p_{\infty})}. \quad (2.6)$$

As for any equation of state, the speed σ of the corresponding fast and slow shocks may be determined from the relations

$$\rho(v - \sigma) = \mp m = \rho_0(v_0 - \sigma), \quad (2.7)$$

where

$$m = \left(- \frac{p - p_0}{1/\rho - 1/\rho_0} \right)^{1/2} \quad (2.8)$$

is the mass flux across the wave.

To demonstrate the adequacy of using a stiffened gas equation of state to model a metal plate made from tungsten we compare to experimental data.¹ These data show that a plot of shock speed $U_s = |\sigma - v_0|$ vs. particle speed $U_p = |v - v_0|$ along the principal Hugoniot of tungsten is well approximated by a straight line

$$U_s \approx c_0 + \alpha U_p \quad (2.9)$$

for pressures up to 3 Mbar. Here $c_0 = 0.404 \text{ cm}/\mu\text{s}$ is (approximately) the sound speed in tungsten at standard conditions and $\alpha = 1.23$ is an empirical dimensionless constant. For a general equation of state one finds from (2.7) and (2.8) that

$$\frac{U_p}{U_s} = \frac{\rho - \rho_0}{\rho}$$

and

$$U_s U_p = \frac{p - p_0}{\rho_0} .$$

Using the Hugoniot relation (2.6) for a stiffened gas, one can eliminate p and ρ to find

$$U_s^2 = \frac{\gamma + 1}{2} U_s U_p + c_0^2$$

so

$$U_s = \left[c_0^2 + \left(\frac{\gamma + 1}{4} U_p \right)^2 \right]^{1/2} + \frac{\gamma + 1}{4} U_p . \quad (2.10)$$

For our calculations modeling tungsten we have used $\gamma = 3.14$ and $p_\infty = 1.0 \text{ Mbar}$. A plot comparing the empirical linear fit to the stiffened gas relation (2.10) for pressures up to 3 Mbar is shown in Fig. 2. The stiffened gas relation coincides with the linear fit to within 3%.

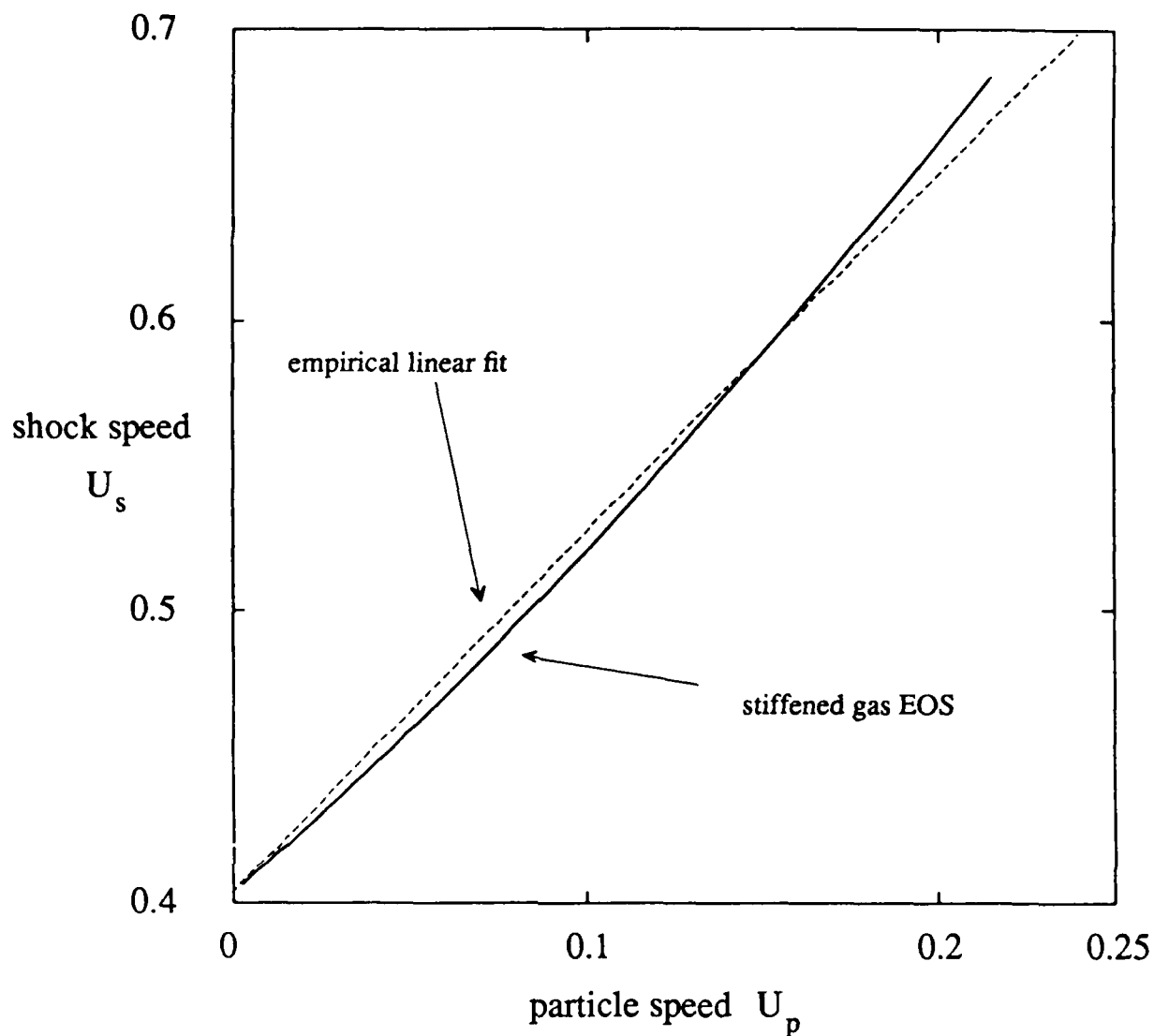


Figure 2. Comparison of the stiffened gas equation of state to experimental data for tungsten. The shock speed U_s along the principle Hugoniot is plotted with respect to the particle speed U_p behind the shock. Speeds are measured in $\text{cm}/\mu\text{s}$, and the range of shock strengths corresponds to overpressures up to 3 Mbar. The stiffened gas is defined by the parameter choices $\gamma = 3.14$ and $p_\infty = 1.0$ Mbar. The comparison shows a maximum difference of 3%.

Riemann Problems

A Riemann problem for a system of conservation laws in one space dimension is an initial-value problem with scale invariant initial data, i.e., data at $t = t_0$ that is constant to either side of a jump discontinuity at $x = x_0$. We use the subscript l to label the initial state on the left of x_0 , and r for the initial state on the right of x_0 . The solution of a Riemann problem is constant along each ray $\xi = (x - x_0)/(t - t_0) = \text{const.}$ through (x_0, t_0) ; thus we may specify the solution as a function of the speed ξ .

The solution of a Riemann problem for a stiffened gas requires only a simple modification of the well-known solution for a polytropic gas. It consists of a slow (i.e., $v - c$) rarefaction or shock wave on the left, a fast (i.e., $v + c$) rarefaction or shock wave on the right, and a contact discontinuity (moving with velocity v) in between, as indicated schematically in Fig. 3. It is convenient to speak of the left side of a slow wave and the right side of a fast wave as being "ahead" of the wave, the opposite sides being "behind" the wave; the corresponding states are labeled by the subscripts a and b . A slow or fast wave is determined by the state ahead of it together with one other parameter, such as the pressure behind it. For the left (resp., right) wave in the solution of a Riemann problem, the state ahead of the wave is the left (resp., right) initial state. Since the particle velocity and the pressure is continuous across a contact discontinuity, the velocities and pressures behind the left and right waves must coincide. Thus solving a Riemann problem amounts to finding the pressure in the middle between the left and right waves such that the particle velocities behind the waves are equal.

For a shock wave, conservation of momentum may be written

$$\mp m(v_a - v_b) + p_a - p_b = 0. \quad (3.1)$$

Here m is defined as a function of the pressure p_b behind the shock and the state ahead of the shock through equations (2.6) and (2.8), so long as $p_b \geq p_a$. For a rarefaction wave, we may define m through the equation

$$-m \cdot \frac{2}{\gamma - 1} (c_a - c_b) + p_a - p_b = 0,$$

so that by (2.3) we find that (3.1) again holds. With this definition and equations (2.4) and (2.2), m may be expressed as a function of p_b and the state ahead of the wave, so long as $p_b < p_a$. More explicitly we have

$$m = (\gamma_a \rho_a (p_a + p_{\infty, a}))^{1/2} \cdot \varphi \left(\frac{p_b + p_{\infty, b}}{p_a + p_{\infty, a}}, \gamma_a \right) \quad (3.2)$$

where

$$\varphi(r, \gamma) = \begin{cases} \frac{\gamma - 1}{2\gamma} \frac{1 - r}{1 - r^{(\gamma-1)/2\gamma}} & \text{if } r < 1 \\ \left(\frac{\gamma + 1}{2\gamma} r + \frac{\gamma - 1}{2\gamma} \right)^{1/2} & \text{if } r \geq 1. \end{cases}$$

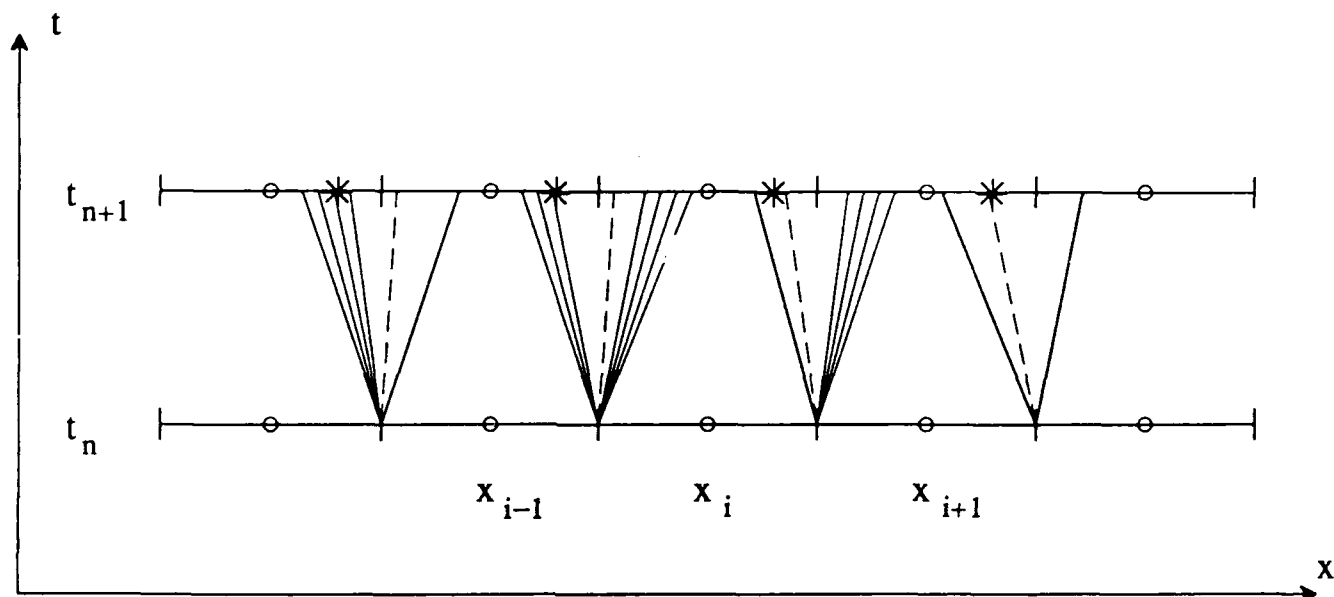


Figure 3. The computational grid for the random choice method. The reconstructed solution is constant in the cells centered on the circles and bounded by the vertical hash marks. The solution of the initial value problem with piecewise constant initial data involves solving a sequence of Riemann problems originating at the boundaries between cells. The solution of a Riemann problem is constant along rays through its origin and, for gas dynamics, consists of a shock or rarefaction wave (indicated by an individual ray or a fan of rays, respectively) on each side of a contact discontinuity (indicated by a dashed ray). The numerical solution after one time step is obtained by sampling the Riemann solutions at the points indicated by the stars, whose shift relative to the cell centers is random in time.

Let v_* and p_* denote the common values of the particle velocity and pressure on the two sides of the contact discontinuity. Then by (3.1) we have

$$-m_r(v_r - v_*) + p_r - p_* = 0$$

and

$$+m_l(v_l - v_*) + p_l - p_* = 0$$

for the right and left waves, where m_r is expressed through (3.2) in terms of $p_b = p_*$ and the density and pressure ρ_r and p_r ahead of the wave, and similarly for m_l . These equations may be written

$$p_* = \frac{v_l - v_r}{1/m_l + 1/m_r} + \frac{m_l p_r + m_r p_l}{m_l + m_r} \quad (3.3)$$

and

$$v_* = \frac{p_l - p_r + m_l v_l + m_r v_r}{m_l + m_r} \quad (3.4)$$

Therefore to solve a Riemann problem we first use the Godunov-Chorin^{6,3} fixed-point iteration to solve (3.3) for the pressure p_* between the left and right waves. Then (3.4) gives the velocity v_* in the middle, and for both the fast and the slow wave the state along a ray moving at a specified speed ξ may be determined using either equations (2.2-5) or equations (2.6-7), according as the wave is a rarefaction or a shock. Except for the modifications to the formulae (2.2), (2.4), (2.6), and (3.2), the construction of the solution of the Riemann problem is identical to that for a polytropic gas (for which $p_\infty = 0$).

Tracked Random Choice Method

The random choice method is a numerical method for solving the general initial-value problem for a system of conservation laws. It is based on the constructive existence proof for solutions of conservation laws of Glimm,⁴ and was adapted for numerical computation by Chorin.³

In the random choice method for the hyperbolic system of conservation laws

$$u_t + f(u)_x = 0 \quad (4.1)$$

the solution is determined at the lattice of space-time points (x_j, t_n) ;

$$x_j = (x_{j-1/2} + x_{j+1/2})/2$$

is the center of the mesh cell from $x_{j-1/2}$ to $x_{j+1/2}$. Given the solution values $u_j^n = u(x_j, t_n)$ at time level n , the solution values u_j^{n+1} at level $n+1$ are determined in three stages.

First, an approximation $u^n(x)$ for the solution at time t_n and an arbitrary position x is reconstructed by defining u^n to be piecewise constant on mesh cells:

$$u^n(x) = u_j^n \quad \text{if} \quad x_{j-1/2} \leq x < x_{j+1/2} \quad (4.2)$$

Next, consider solving the initial-value problem for (4.1) with initial data (4.2) at time t_n . For $t - t_n$ sufficiently small, the solution is given in terms of the solutions of a sequence of Riemann problems between the states u_j^n and u_{j+1}^n and centered at the points $(x_{j+1/2}, t_n)$. The situation is depicted in Fig. 3. In fact, the waves in the solutions of the Riemann problems centered at neighboring points $(x_{j-1/2}, t_n)$ and $(x_{j+1/2}, t_n)$ will not interact so long as the Courant-Friedrichs-Levy condition

$$t - t_n < t_{\text{CFL}} = \frac{1}{2} \min_j (x_{j+1/2} - x_{j-1/2}) / \lambda_j \quad (4.3)$$

holds, where λ_j is the maximum wave speed, in absolute value, in the solution of the Riemann problem centered at $(x_{j+1/2}, t_n)$. We have taken $t_{n+1} - t_n = C \cdot t_{\text{CFL}}$ with the Courant number C kept between 0.7 and 0.9.

Finally, an equidistributed random number η_{n+1} is chosen from the interval

$$-1/2 \leq \eta_{n+1} < 1/2,$$

and the solution value u_j^{n+1} is taken to be the value u_* of the solution of the above initial-value problem sampled at the position

$$x_* = x_j + \eta_{n+1} \cdot (x_{j+1/2} - x_{j-1/2})$$

at time t_n . In our computations we have used the Van der Corput sequence³ to obtain η .

The solution given by the random choice method has the advantage, when compared to standard finite difference methods, of preserving the structure of discontinuous waves in

the solution: shock waves and contact discontinuities remain perfectly sharp. The method is therefore able to detect formation of shock waves within regions extending only a few mesh cells. This property is crucial for our application to shockless acceleration of thin plates.

The price paid for perfect resolution of discontinuous waves is that their positions are not exactly correct. On the average the position of a discontinuous wave in the numerical solution is correct, but the wave performs a random walk about this correct position. To remedy this in situations where maintaining the position of certain prominent waves is critical, Glimm, Marchesin, and McBryan introduced the tracked random choice method.⁵

In a front tracking method, certain waves in the flow, typically strong discontinuous waves, are resolved on a subgrid level. With each tracked front is associated a position and a wave type. The wave type determines how the tracked front moves and interacts with the fluid. For example, in gas dynamics the possible wave types include slow and fast pressure waves and contact discontinuities.

Let x_f^n denote the position of a particular tracked front at time t_n . If the tracked front lies in the j^{th} mesh cell at time t_n , i.e., $x_{j-1/2} \leq x_f^n < x_{j+1/2}$, then the solution values u_{j-1}^{n+1} , u_j^{n+1} , and u_{j+1}^{n+1} are obtained in a fashion different from that just described. The piecewise constant data u^n is defined by

$$u^n(x) = \begin{cases} u_{j-1}^n & \text{if } x_{j-3/2} \leq x < x_f^n \\ u_{j+1}^n & \text{if } x_f^n \leq x < x_{j+3/2} \end{cases}$$

for x in the interval $x_{j-3/2} \leq x < x_{j+3/2}$, and by (4.2) for x outside this interval. As before, the initial-value problem with initial data u^n at time t_n is solved up to time t_{n+1} . The position of the tracked front at time t_{n+1} is

$$x_f^{n+1} = x_f^n + s \cdot (t_{n+1} - t_n),$$

where the velocity s is determined according to its wave type. Finally, the solution value u_{j-1}^{n+1} is taken to be the value u_* of the solution of this initial-value problem at time t_{n+1} sampled at the position

$$x_* = x_{j-3/2} + (\eta_{n+1} + 1/2) (x_f^{n+1} - x_{j-3/2}).$$

Similarly u_{j+1}^{n+1} is obtained by sampling at

$$x_* = x_f^{n+1} + (\eta_{n+1} + 1/2) (x_{j+3/2} - x_f^{n+1}).$$

The choice for the value of u_j^{n+1} seems somewhat arbitrary. For instance, one could take u_j^{n+1} to be u_{j-1}^{n+1} or u_{j+1}^{n+1} according as $x_j \leq x_f^{n+1}$ or $x_f^{n+1} < x_j$. We have found that with this choice, however, a strong wave crossing the tracked wave does not separate correctly from the tracked wave after the interaction. This effect is rather dramatic in calculations where a tracked shock wave is followed closely by a strong rarefaction wave. To remedy this we instead define u_j^{n+1} to be u_{f-}^{n+1} or u_{f+}^{n+1} according as $x_j \leq x_f^{n+1}$ or $x_f^{n+1} < x_j$, where u_{f-}^{n+1} and u_{f+}^{n+1} are the states on either side of the tracked front.

In gas dynamics the possible wave types are: contact discontinuities, moving with the particle velocity v ; slow and fast pressure waves, which either follow sound waves moving with velocity $v \pm c$ in case the solution is continuous across the wave (the rarefaction case), or move with the shock velocity σ if the wave is discontinuous (the shock case); Neumann and Dirichlet boundaries, which supply boundary conditions; and movable walls, which are ascribed a mass density and move according to Newton's law. The velocity of a slow or fast pressure wave or contact discontinuity, is calculated by solving the Riemann problem between u_{j-1}^n and u_{j+1}^n , centered at (x_f^n, t_n) , and determining the velocity of the corresponding wave in this solution. (We track the leading edge of a rarefaction wave.) Neumann and Dirichlet boundaries are stationary, and their interaction with the flow is determined by solving a Riemann problem between the fluid state neighboring the boundary and, respectively, the same state with a reflected velocity or the imposed boundary state. The evolution of a movable wall is determined as follows.

Let the wall have mass per unit area M and velocity v_{wall}^n at time t_n . Suppose for concreteness that the fluid lies on the right side of the wall, so that the solution value inside the fluid is $u_r = u_{j+1}^n$. Define the virtual state u_l to have the same pressure and density as u_r , and to have the velocity

$$v_l = 2v_{\text{wall}}^n - v_r$$

obtained by reflection through the moving wall. Then solve the Riemann problem between u_l and u_r centered at (x_f^n, t_n) and sample it at the position

$$x_* = x_f^n + v_{\text{wall}}^n \cdot (t_{n+1} - t_n)$$

to obtain the state u_* on the fluid side of the wall at time t_{n+1} . Because v_l is obtained by reflection, the velocity v_* of the fluid at the wall coincides with v_{wall}^n , so that the correct boundary conditions have been maintained. The pressure in the fluid accelerates the movable wall according to Newton's law. If $\Delta t = t_{n+1} - t_n$ is small enough (more precisely, as may be deduced from the analytic solution,⁹ if $p_* \Delta t / Mc_*$ is small) we may approximate this acceleration by

$$v_{\text{wall}}^{n+1} = v_{\text{wall}}^n + \frac{p_r + p_*}{2} \cdot \frac{\Delta t}{M}.$$

The speed s of the moving wall during this time interval is then taken to be

$$s = \frac{1}{2} (v_{\text{wall}}^{n+1} + v_{\text{wall}}^n).$$

To obtain acceptable resolution of the waves in the thin plate the computational grid must be refined in the vicinity of the plate. The positions of the the edges of the mesh cells $x_{j+1/2}$, $j = 0, \dots, N$ are defined as follows. The grid spans the interval $[x_{\min}, x_{\max}]$ and has a subinterval $[a, b]$ over which the mesh is refined by the refinement ratio R . To smooth the transition between the coarse and fine meshes, a molification parameter ϵ is also specified, with $\epsilon = 0$ corresponding to a sharp transition. We define

$$\rho_0(\xi) = \begin{cases} 1/R & \text{if } 0 < \xi < 1 \\ 1 & \text{otherwise} \end{cases} \quad (4.4)$$

and let ρ_ϵ be the convolution $\rho_\epsilon = \delta_\epsilon * \rho_0$ of ρ_0 with an approximate δ -function. We have used

$$\delta_\epsilon(\xi) = \frac{1}{\epsilon} \delta_1\left(\frac{\xi}{\epsilon}\right)$$

where

$$\delta_1(\xi) = \frac{1}{\pi(1+\xi^2)}.$$

With these definitions, the zone edges are given by

$$x_{j+1/2} = x_{\min} + (x_{\max} - x_{\min}) \cdot \frac{\int_{\xi_0}^{\xi_j} d\xi \rho_\epsilon(\xi)}{\int_{\xi_0}^{\xi_N} d\xi \rho_\epsilon(\xi)} \quad (4.5)$$

where

$$\xi_j = \xi_0 + \frac{j}{N} \cdot (\xi_N - \xi_0).$$

It remains to define ξ_0 and ξ_N . The transitions occurring between the coarse and fine meshes at $\xi = 0$ and $\xi = 1$ in (4.4) are to correspond to $x = a$ and $x = b$ through (4.5). For $\epsilon \neq 0$ this gives a pair of nonlinear equations to be solved for ξ_0 and ξ_N in terms of a and b . When $\epsilon = 0$, however, these equations reduce to linear equations, with the solution

$$\xi_0 = -\frac{1}{R} \frac{a - x_{\min}}{b - a}$$

and

$$\xi_N = 1 + \frac{1}{R} \frac{x_{\max} - b}{b - a};$$

for simplicity we use these equations to define ξ_0 and ξ_N .

Analytical Results

As a preliminary to solving the shockless acceleration problem, we study a similar problem for which analytical information is available. This is the problem of the reflection from a rigid wall of a rarefaction wave expanding into a vacuum. The short-time asymptotic solution of this problem has been described by Greenspan and Butler;⁷ they reduce the problem to the solution of a boundary-value problem for a system of ordinary differential equations, which they solve numerically. These equations may, in fact, be integrated analytically, and we describe this solution here.

The flow pattern is shown in Fig. 4. A rarefaction wave in a polytropic gas with adiabatic exponent γ connects the state $\rho = \rho_0$, $p = p_0$, $v = v_0$ to the vacuum $\rho = 0$, $p = 0$; it originates at $x = 0$ at time $t = 0$. The rarefaction wave corresponds to the slow (i.e., $v - c$) family of characteristics, so within the wave the fluid state is

$$\begin{aligned} \rho &= \rho_0 (c/c_0)^{2/(\gamma-1)}, \\ p &= p_0 (c/c_0)^{2\gamma/(\gamma-1)}, \\ v &= v_0 + \frac{2}{\gamma-1} (c_0 - c), \end{aligned} \quad (5.1)$$

where

$$c = \frac{\gamma-1}{\gamma+1} \left(v_0 + \frac{2}{\gamma-1} c_0 - \frac{x}{t} \right),$$

by virtue of Eqs. 2.2-5. Since the tail of the wave corresponds to $c = 0$, the rarefaction arrives at the wall located at $x = x_0$ at time

$$t_0 = x_0 \left(v_0 + \frac{2}{\gamma-1} c_0 \right)^{-1}.$$

At this time a reflected shock wave forms to decelerate the expanding fluid.

Following Greenspan and Butler we seek a scaling solution for the flow between the reflected shock and the wall in terms of the variables $\tau = t - t_0$ and $\xi = (x - x_0)/(t - t_0)$. Ahead of the reflected wave the state is given by Eqs. 5.1, where c may be written

$$c = \frac{\gamma-1}{\gamma+1} (\xi_0 - \xi) \frac{\tau}{t_0 + \tau}$$

with $\xi_0 = x_0/t_0$. Thus the state just ahead of the reflected shock wave satisfies $\rho_a = O((\tau/t_0)^{2/(\gamma-1)})$, $p_a = O((\tau/t_0)^{2\gamma/(\gamma-1)})$, and $v_a = O(1)$ as $\tau \rightarrow 0$. The state $\rho = \rho_b$, $p = p_b$, $v = v_b$ just behind the reflected shock wave must satisfy the Hugoniot relation Eq. 2.6 together with

$$(v_b - v_a)^2 = (p_b - p_a) (1/\rho_a - 1/\rho_b), \quad (5.2)$$

which is a consequence of momentum conservation. Assuming a non-negligible part of the deceleration of the fluid occurs across the shock wave, so that its strength does not vanish as $\tau \rightarrow 0$, the left-hand side of this last equation is $O(1)$. It follows that

$$p_b = O\left((\tau/t_0)^{2\gamma/(\gamma-1)}\right)$$

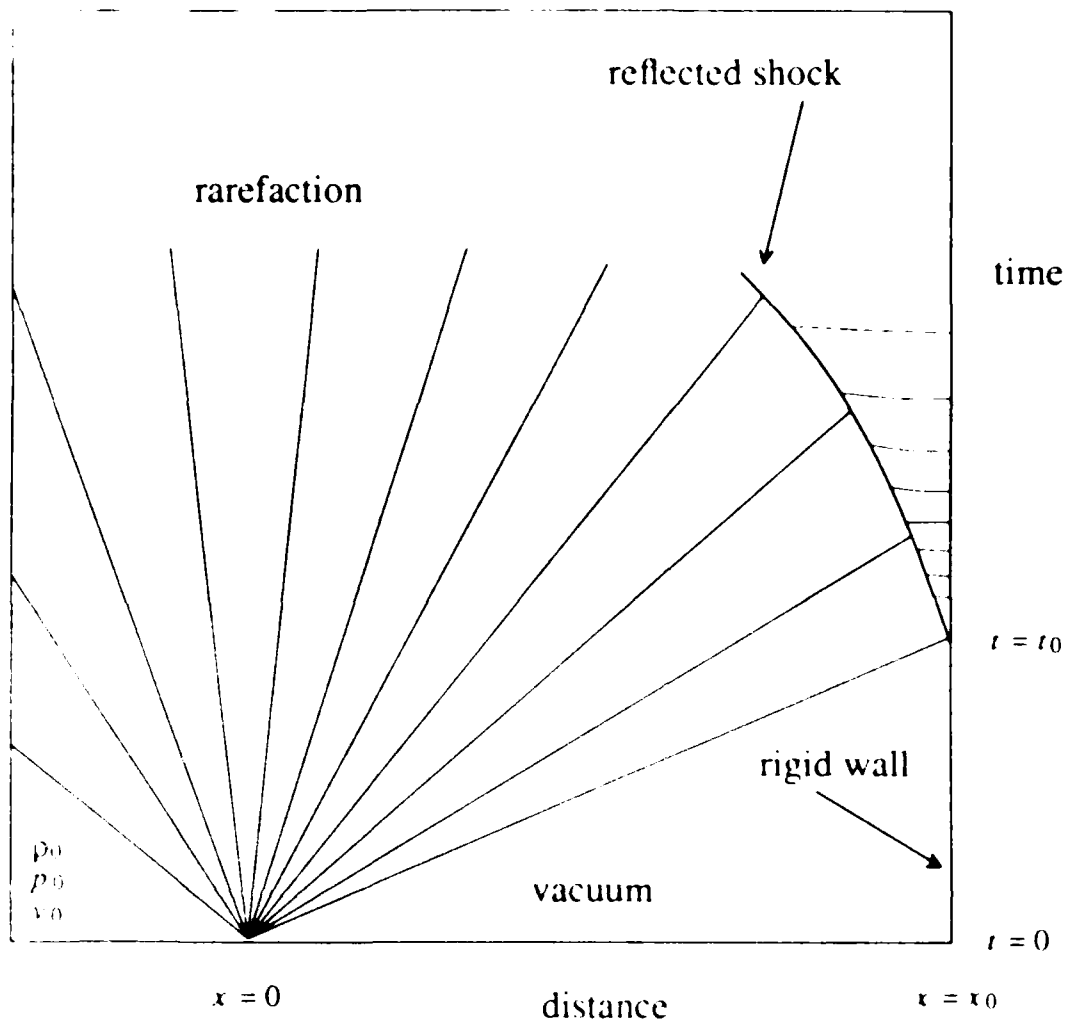


Figure 4. Reflection of a rarefaction from a rigid wall. A rarefaction wave in a polytropic gas connects the state with $\rho = \rho_0$, $p = p_0$, and $v = v_0$ to a vacuum state. The rarefaction originates at $x = 0$, and its tail strikes a rigid wall at $x = x_0$ at time $t = t_0$, whereupon a reflected shock is formed.

and hence that

$$\rho_b = \frac{\gamma + 1}{\gamma - 1} \rho_a \cdot (1 + O(\tau/t_0)^2)$$

as $\tau \rightarrow 0$. Thus the reflected shock is infinite in strength at the time of its formation.

In this way, Greenspan and Butler are led to expect that the solution between the reflected shock wave and the wall is, asymptotically as $\tau \rightarrow 0$, of the form

$$\begin{aligned} \rho &= (\tau/t_0)^{2/(\gamma-1)} \hat{\rho}(\xi), \\ p &= (\tau/t_0)^{2/(\gamma-1)} \hat{p}(\xi), \\ v &= \hat{v}(\xi); \end{aligned} \quad (5.3)$$

here ξ lies in the range $\sigma_0 < \xi < 0$, σ_0 being the limiting velocity of the reflected shock wave as $\tau \rightarrow 0$. By assuming that the solution is of this form, they find a system of nonlinear ordinary differential equations to be satisfied by $\hat{\rho}$, \hat{p} , and \hat{v} , and they solve the equations numerically. However, one can find an analytic solution of these equations in terms of incomplete beta functions, as we now show.

The flow is governed by the characteristic equations

$$\begin{aligned} v_t \pm \frac{1}{\rho c} p_t + (v \pm c) \left(v_x \pm \frac{1}{\rho c} p_x \right) &= 0, \\ p_t - c^2 \rho_t + v (p_x - c^2 \rho_x) &= 0. \end{aligned}$$

It is subject to no-flow boundary conditions $v = 0$ at $\xi = 0$, and to the boundary conditions

$$\begin{aligned} v &= v_b = \sigma_0 + \frac{\gamma - 1}{\gamma + 1} (\xi_0 - \sigma_0), \\ c &= c_b = \frac{\sqrt{2\gamma(\gamma - 1)}}{\gamma + 1} (\xi_0 - \sigma_0), \end{aligned}$$

and

$$\hat{p} = \hat{p}_b = p_0 \cdot \frac{2\gamma}{\gamma + 1} \left(\frac{\gamma - 1}{\gamma + 1} \right)^{2/(\gamma-1)} \left(\frac{\xi_0 - \sigma_0}{c_0} \right)^{2\gamma/(\gamma-1)},$$

at $\xi = \sigma_0$; these conditions follow from mass conservation, Eq. 2.7, and momentum conservation, Eq. 5.2, in the strong-shock limit.

Upon substituting the polytropic gas relation $c^2 = \gamma p / \rho$, the characteristic equations may be written

$$\left(v_t \pm \frac{2}{\gamma - 1} c \right)_t + (v \pm c) \left(v_x \pm \frac{2}{\gamma - 1} c \right)_x - c \left(\frac{2}{\gamma - 1} c_x - \frac{1}{\rho c} p_x \right)$$

and

$$\frac{1}{\rho c} p_t - \frac{2}{\gamma - 1} c_t + v \left(\frac{1}{\rho c} p_x - \frac{2}{\gamma - 1} c_x \right) = 0$$

When the solution is assumed to be of the form of Eq. 5.3, $v = \hat{v}$ and $c = \hat{c} = (\gamma \hat{p} / \hat{\rho})^{1/2}$ are independent of r , so the last equation becomes

$$\frac{2}{\gamma-1} \hat{c}' - \frac{1}{\hat{\rho} \hat{c}} \hat{p}' = \frac{2}{\gamma(\gamma-1)} \frac{\hat{c}}{\hat{v} - \xi}; \quad (5.4)$$

therefore the previous pair of equations reads

$$(\hat{v} \pm \hat{c} - \xi) \left(\hat{v}' \pm \frac{2}{\gamma-1} \hat{c}' \right) = \frac{2}{\gamma(\gamma-1)} \frac{\hat{c}^2}{\hat{v} - \xi}, \quad (5.5)$$

where the prime denotes differentiation with respect to ξ .

In terms of $c = \hat{c}$ and the Mach number $M = (v - \xi)/c$, Eqs. 5.5 are

$$M(M \pm 1) \left[1 + cM' + \left(M \pm \frac{2}{\gamma-1} \right) c' \right] = \frac{2}{\gamma(\gamma-1)},$$

i.e.,

$$cM' = -\frac{1}{2\gamma\epsilon} (1 - 2\gamma\epsilon M^2) (1 - M^2)^{-1} \quad (5.6)$$

and

$$Mc' = \frac{1}{\gamma} (1 - M^2)^{-1}, \quad (5.7)$$

while Eq. 5.4, when combined with Eq. 5.7, becomes

$$c \frac{\hat{p}'}{\hat{p}} = \frac{2}{\gamma-1} M (1 - M^2)^{-1}.$$

We have introduced the parameter $\epsilon = \frac{1}{2}(\gamma-1)/(\gamma^2+1)$ for later convenience.

The ratio of Eqs. 5.6 and 5.7 dictates that

$$\frac{dM^2}{d \log c} = -\frac{1}{\epsilon} (1 - 2\gamma\epsilon M^2) \cdot M^2,$$

which integrates to yield

$$c = c_b \left(\frac{M_b^2 (1 - 2\gamma\epsilon M^2)}{M^2 (1 - 2\gamma\epsilon M_b^2)} \right)^\epsilon \quad (5.8)$$

Here $M_b = (v_b - \sigma_0)/c_b$, $\sqrt{(\gamma-1)/2\gamma}$ is the Mach number just behind the reflected shock wave. Similarly,

$$\frac{dM^2}{d \log \hat{p}} = \frac{\gamma-1}{2\gamma\epsilon} (1 - 2\gamma\epsilon M^2),$$

so

$$\hat{p} = \hat{p}_b \left(\frac{1 - 2\gamma\epsilon M^2}{1 - 2\gamma\epsilon M_b^2} \right)^{1/(1-\epsilon)} \quad (5.9)$$

By using Eq. 5.8, Eq. 5.6 may be written

$$(1 - M^2) (1 - 2\gamma\epsilon M^2)^{-(1-\epsilon)} (M^2)^{-(\frac{1}{2}+\epsilon)} dM^2 = -\frac{1}{\gamma\epsilon} \left(\frac{1 - 2\gamma\epsilon M_b^2}{M_b^2} \right)^\epsilon \frac{d\xi}{c_b}.$$

Consequently, if we define

$$\psi_\gamma(y) = \int_0^y (1-z)(1-2\gamma\epsilon \cdot z)^{-(1-\epsilon)} z^{-(\frac{1}{2}+\epsilon)} dz$$

(where, again, $\epsilon = \frac{1}{2}(\gamma - 1)/(\gamma^2 + 1)$), then

$$\psi_\gamma(M_b^2) - \psi_\gamma(M^2) = \frac{1}{\gamma\epsilon} \left(\frac{1 - 2\gamma\epsilon M_b^2}{M_b^2} \right)^\epsilon \frac{\xi - \sigma_0}{c_b}. \quad (5.10)$$

Since ψ_γ is a monotone function, Eq. 5.10 may be solved for M^2 in terms of ξ , which gives c and \hat{p} as functions of ξ through Eqs. 5.8 and 5.9. Furthermore, by imposing the boundary condition that $M = 0$ at $\xi = 0$, we obtain an equation for σ_0/ξ_0 as a function of γ :

$$\frac{U_s}{v_0 + 2c_0/(\gamma - 1)} = -\frac{\sigma_0}{\xi_0} = \left[\frac{1}{\gamma\epsilon} \frac{\gamma + 1}{\sqrt{2\gamma(\gamma - 1)}} \frac{1}{\psi_\gamma(M_b^2)} \left(\frac{1 - 2\gamma\epsilon M_b^2}{M_b^2} \right)^\epsilon - 1 \right]^{-1}. \quad (5.11)$$

Notice that the function ψ_γ may be expressed in terms of incomplete beta functions, which are defined by

$$B(p, q; y) = \int_0^y z^{p-1} (1-z)^{q-1} dz$$

when p and q have positive real parts. In fact,

$$\psi_\gamma(y) = (2\gamma\epsilon)^{-(\frac{1}{2}-\epsilon)} B(\frac{1}{2} - \epsilon, \epsilon; 2\gamma\epsilon y) - (2\gamma\epsilon)^{-(\frac{1}{2}-\epsilon)} B(\frac{3}{2} - \epsilon, \epsilon; 2\gamma\epsilon y).$$

For $1 \leq \gamma < \infty$, ϵ is bounded by $0 \leq \epsilon \leq [4(1 + \sqrt{2})]^{-1} = 0.10355 \dots$, so ψ_γ is well-defined.

To confirm these analytical results, and to demonstrate of the accuracy of the random choice method, Fig. 5 shows a comparison of the analytical results with the results of solving the partial differential equations governing the rarefaction reflection flow. In this problem, a rarefaction wave connecting a pressure $p_0 = 1$ and density $\rho_0 = 1$ to a vacuum expands from $x = 0$ and strikes a rigid wall at $x = x_0 = 1$ at time $\tau = 0$; the fluid is a polytropic gas with $\gamma = 1.4$. Two calculations were performed, one a free expansion for which $v_0 = 0$, and one in which the expanding material has been shocked to $v_0 = \sqrt{2/\gamma(\gamma - 1)}c_0$, which corresponds to an infinite-strength shock. The short-time asymptotic solution predicts that the pressure at the wall should rise as $(\tau/t_0)^{2/(\gamma-1)}$ and that the speed of the reflected shock should tend to $U_s = 0.036494 \cdot (v_0 + 2c_0/(\gamma - 1))$. In this computation, the flow in the region $0.9 < x < 1$ and $0 < \tau < 0.3$ was simulated using 100 mesh cells. Fig. 5 shows the agreement with the asymptotic pressure rise, and a contour plot of pressure in the

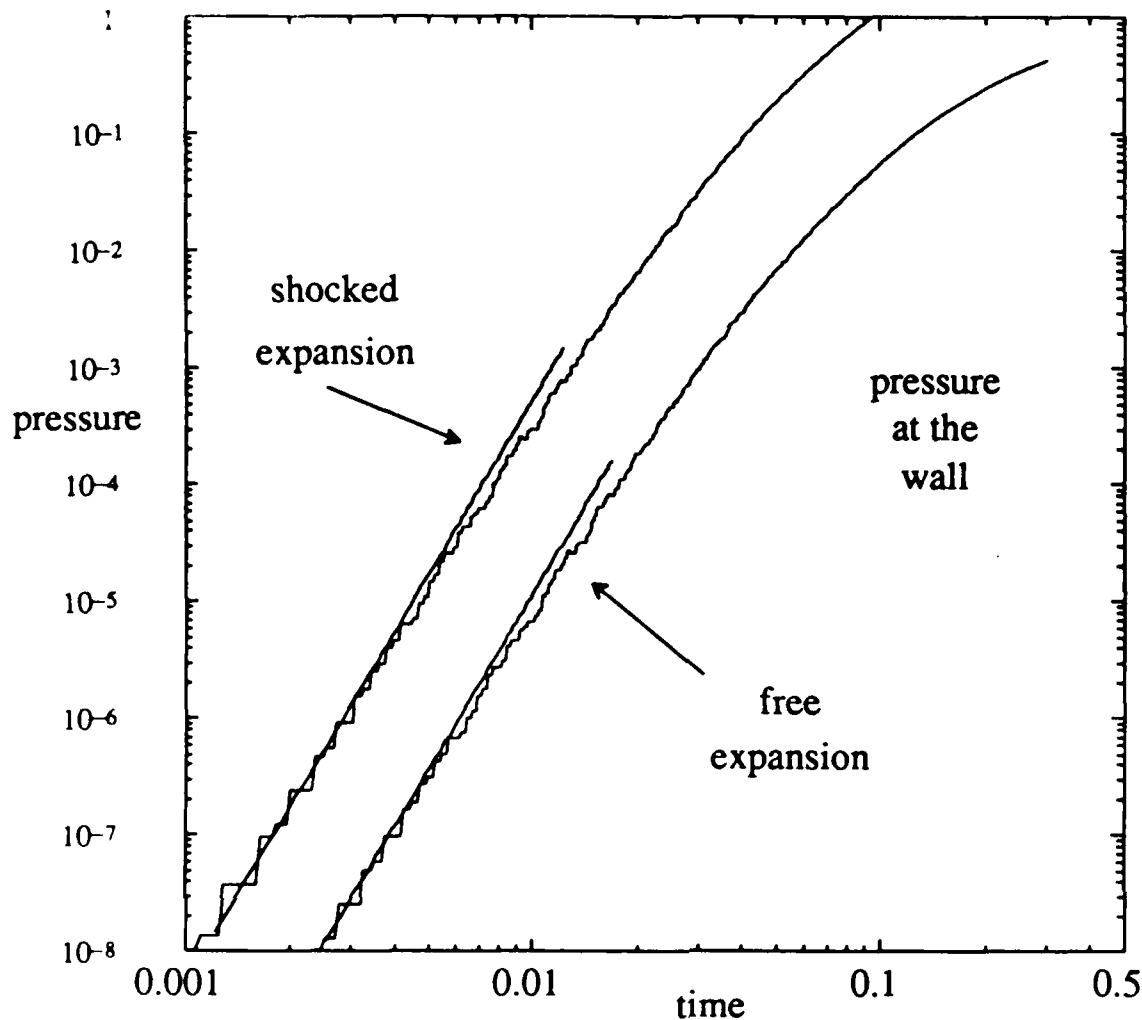


Figure 5. Pressure at the wall for the reflection of a rarefaction wave expanding into a vacuum. The pressure at the rigid wall, plotted as a function of time, is shown for two sets of initial conditions. In both cases the initial density and pressure in the expanding material are $\rho_0 = 1$ and $p_0 = 1$. For the free expansion, the initial velocity is $v_0 = 0$, whereas for the shocked expansion v_0 corresponds to driving the expanding material with an infinite-strength shock. In these computations, the rarefaction wave originates at $x = 0$, and the flow in the region $0.9 \leq x \leq 1$ and $0 \leq t \leq 0.3$ was simulated using 100 mesh cells. Superimposed are the short-time asymptotic solutions, which appear as straight lines. Both solutions confirm the predicted short-time asymptotic behavior of the pressure, *viz.*, that it should rise as t^5 when $\gamma = 1.4$. Also, the solutions are accurate over 8 decades in pressure, in contrast to other numerical methods.

space-time plane shows that the reflected shock speed agrees as well. One may ascertain that the short-time asymptotic solution is valid for $\tau/t_0 < 0.1$, roughly speaking.

We point out that the random choice solution is accurate over more than 8 decades in pressure; this contrasts with serious discrepancies, over only 3 decades in pressure, among several numerical methods applied to this problem, as reported by McCall.¹⁰

Suppose now that the wall is replaced with a thin metallic plate that is allowed to accelerate. The behavior of the pressure at the plate is the same as for a rigid wall until the plate has accelerated significantly. The rising pressure generates a compressive wave inside the plate, and we wish to determine whether this wave collapses into a shock wave within the plate.

Simple geometry shows that the sound characteristics inside the plate will cross within the plate if

$$\delta x = \frac{c^2}{dc/dt}$$

is less than the thickness of the plate. If the plate is modeled as a stiffened gas with adiabatic exponent γ_0 , then

$$\delta x = \frac{2\gamma_0}{\gamma_0 - 1} c \cdot \frac{p + p_\infty}{dp/dt} \quad (5.12)$$

because the flow is isentropic. According to Eq. 5.3,

$$\frac{dp}{dt} = \frac{2}{\gamma - 1} \frac{p}{\tau},$$

so in the limit $p \ll p_\infty$,

$$\begin{aligned} \delta x &= \frac{2\gamma_0}{\gamma_0 - 1} c_\infty \left(\frac{p + p_\infty}{p_\infty} \right)^{(\gamma_0 - 1)/2\gamma_0} \cdot \frac{\gamma - 1}{2} \frac{p + p_\infty}{p} \tau \\ &\approx c_\infty t_0 \cdot \gamma_0 \frac{\gamma - 1}{\gamma_0 - 1} \frac{p_\infty}{\hat{p}(0)} \left(\frac{\tau}{t_0} \right)^{-(3-\gamma)/(\gamma-1)}, \end{aligned}$$

where c_∞ denotes the sound speed in the plate at zero pressure.

When $\gamma = 5/3$ and the propellant material has been shocked with an infinite-strength shock, $\hat{p}(0) = 51.678 p_0$ by the results above. Therefore if we consider tungsten ($c_\infty = 0.404 \text{ cm}/\mu\text{s}$, $\gamma_0 = 3.14$, $p_\infty = 1 \text{ Mbar}$) accelerated by plastic foam that has been shocked to $p_0 = 0.24 \text{ Mbar}$ and $\rho_0 = 0.12 \text{ g}/\text{cm}^3$ and that is separated from the plate by a 5 cm gap, one calculates that $\delta x > 0.5 \text{ cm}$ during the initial stages of the acceleration, $\tau < 0.1 t_0 \approx 0.06 \mu\text{s}$. This agrees with the estimate given by McCall.¹⁰

Computational Results

In Figs. 6-9 are shown the results of a shockless acceleration experiment in which the cavity has been evacuated to 10^{-4} bar (the remaining fluid being a gas with $\gamma = 5/3$). The foam, which is modeled as a polytropic gas with $\gamma = 5/3$, is initially at atmospheric pressure and density 0.03 g/cm^3 . The foam is then shocked to 0.24 Mbar and 0.12 g/cm^3 ; the particle velocity in the shocked foam is $2.45 \text{ cm}/\mu\text{s}$.

In this computation the tungsten plate is tracked, with the plate modeled as a movable wall with an areal mass density of 0.5 g/cm^2 , corresponding to a thickness of 0.025 cm. A 3:1 mesh refinement is used for $4 < x < 6 \text{ cm}$, with a total of 300 mesh cells: the mesh spacing near $x = 5 \text{ cm}$ is $\Delta x \approx 0.013 \text{ cm}$, while near $x = 10 \text{ cm}$ it is $\Delta x \approx 0.035 \text{ cm}$.

Figs. 6 and 7 show the space-time development of the flow in terms of the contours of density and pressure, respectively. At time $t = 0$ the shock reaches the end of the foam at $x = 0$, whereupon the foam expands into the cavity. A very weak shock, which is not visible in these plots, is transmitted into the gas in the cavity and leads the expanding foam; its arrival at the tungsten plate is indicated in the figures. The foam decelerates when it strikes the plate, so a reflected shock forms and strengthens. The increasing pressure in the foam that builds up behind the plate serves to accelerate the plate.

The pressure behind the tungsten plate is plotted as a function of time in Fig. 8. Because the cavity has been evacuated, the pressure rise is much smoother than if no cavity had been there. The velocity of the tungsten plate is plotted as a function of time in Fig. 9. The velocity of the plate at $t = 3.85 \mu\text{s}$ is $2.69 \text{ cm}/\mu\text{s}$.

Fig. 8 may be used to obtain another estimate for the crossing distance for characteristics in the plate. The rate of pressure rise is estimated from the graph to be $dp/dt \approx 1.1 \text{ Mbar}/\mu\text{s}$, so Eq. 5.12 gives

$$\delta x > \frac{2\gamma_0}{\gamma_0 - 1} c_\infty \cdot \frac{p_\infty}{dp/dt} \approx 1 \text{ cm},$$

which is 40 times the thickness of the plate.

In Figs. 10-13 are shown the results of a shockless acceleration experiment in which the cavity is filled with air (with $\gamma = 5/3$) at standard conditions. The foam is shocked as in the previous computation. In this computation, both the foam-air contact and the tungsten plate are tracked. The tungsten plate is modeled as a movable wall with an areal mass density of 0.5 g/cm^2 . A 3:1 mesh refinement is used for $4 < x < 6 \text{ cm}$, as before.

Figs. 10 and 11 show the space-time contours of density and pressure, respectively. At time $t = 0$ the shock reaches the end of the foam at $x = 0$, whereupon the foam expands into the cavity and compresses the air, thereby accelerating the tungsten plate. Because the cavity is not evacuated, the weak shock that is transmitted to the air has more noticeable effects; its arrival at the plate is marked by a shock reflected from the plate. The contact discontinuity between the foam and the air interacts with waves reflected from the plate, which strengthen into a reflected shock that overtakes the expansion wave in the foam. A layer of compressed air moving with the plate separates the foam from the plate.

There is much more structure in the flow near the plate in this computation as compared to the previous one. The succession of shock waves reflecting between the foam-air contact discontinuity and the tungsten plate can clearly be seen by comparing Figs. 10

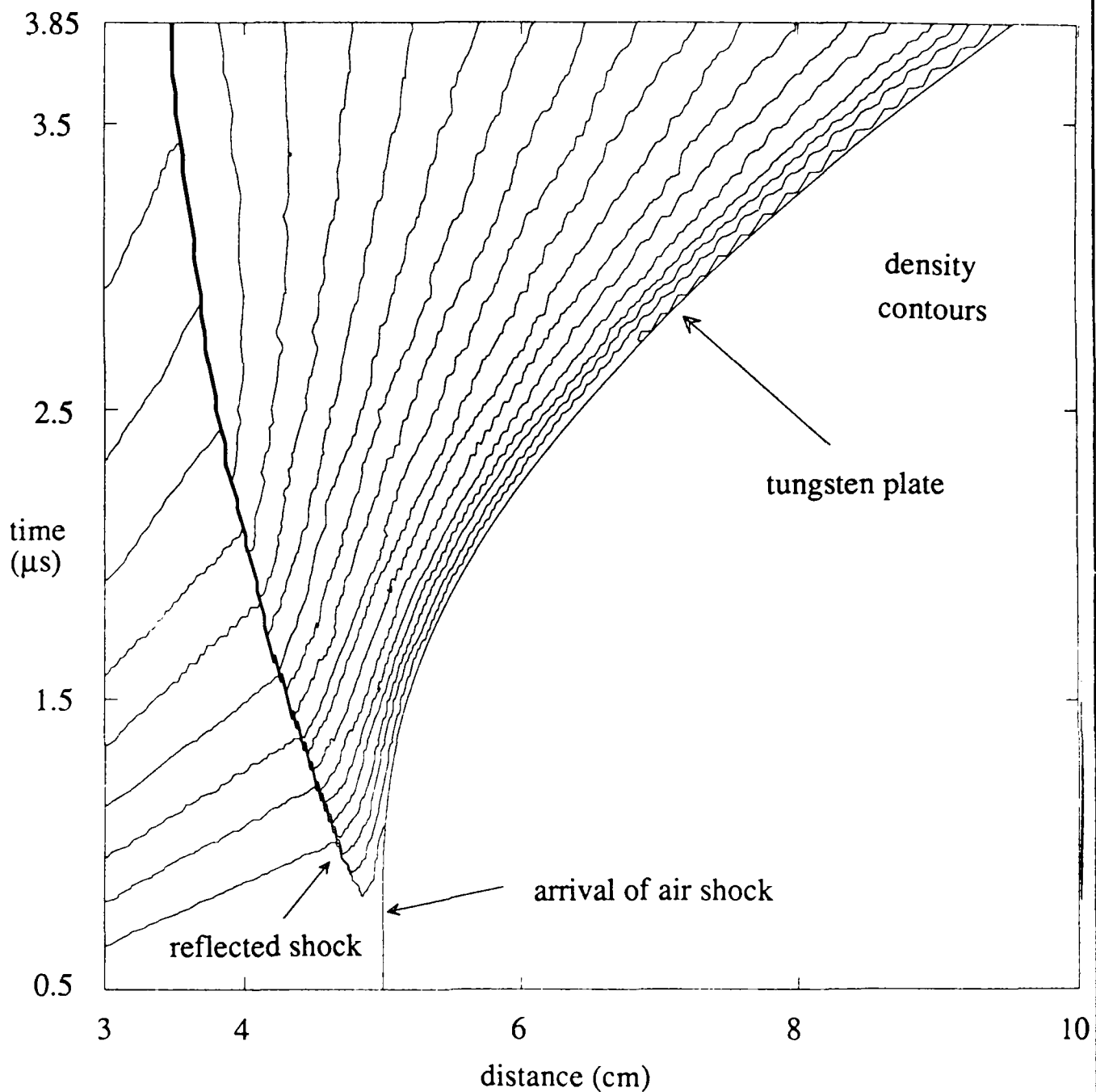


Figure 6. Density contours for shockless acceleration using an evacuated cavity. The foam, initially at atmospheric pressure and density 0.03 g/cm^3 , is shocked to 0.24 Mbar and 0.12 g/cm^3 ; the particle velocity in the shocked foam is $2.45 \text{ cm}/\mu\text{s}$. At time $t = 0$ the shock reaches the end of the foam at $x = 0$, whereupon the foam expands into the cavity, which is evacuated to 10^{-4} bar ; the expanding foam accelerates a tungsten plate. A reflected shock forms in the rarefied foam upon its arrival at the plate. The velocity of the plate at the $t = 3.85 \mu\text{s}$ is $2.69 \text{ cm}/\mu\text{s}$. In this computation the tungsten plate is tracked, with the plate modeled as a movable wall with an areal mass density of 0.5 g/cm^2 . A 3:1 mesh refinement is used for $4 < x < 6 \text{ cm}$, with a total of 300 mesh cells: the mesh spacing near $x = 5 \text{ cm}$ is $\Delta x \approx 0.013 \text{ cm}$, while near $x = 10 \text{ cm}$ it is $\Delta x \approx 0.035 \text{ cm}$.

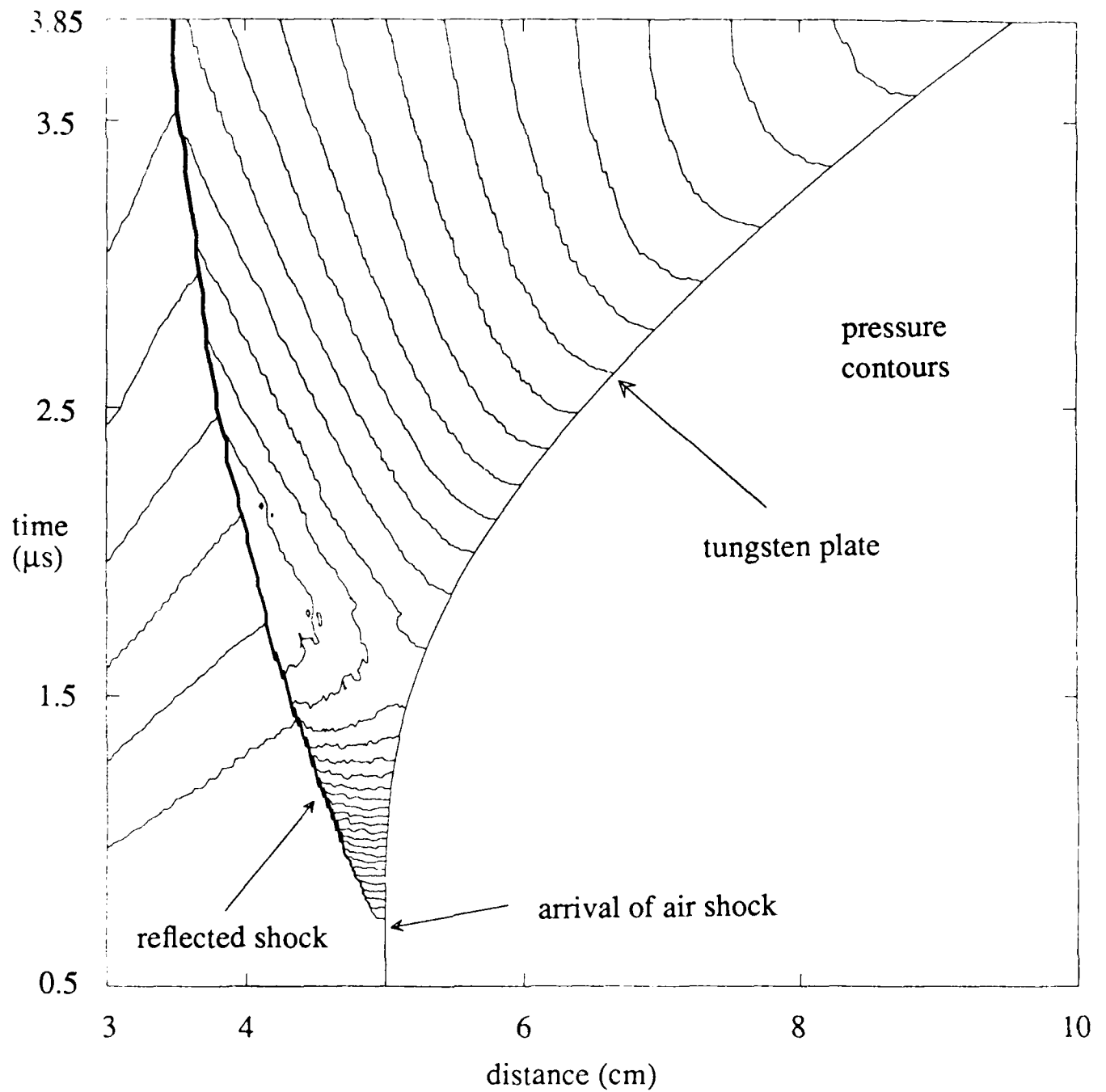


Figure 7. Pressure contours for shockless acceleration using an evacuated cavity. The space-time contours of pressure are shown for the computation described in the caption for Fig. 6.

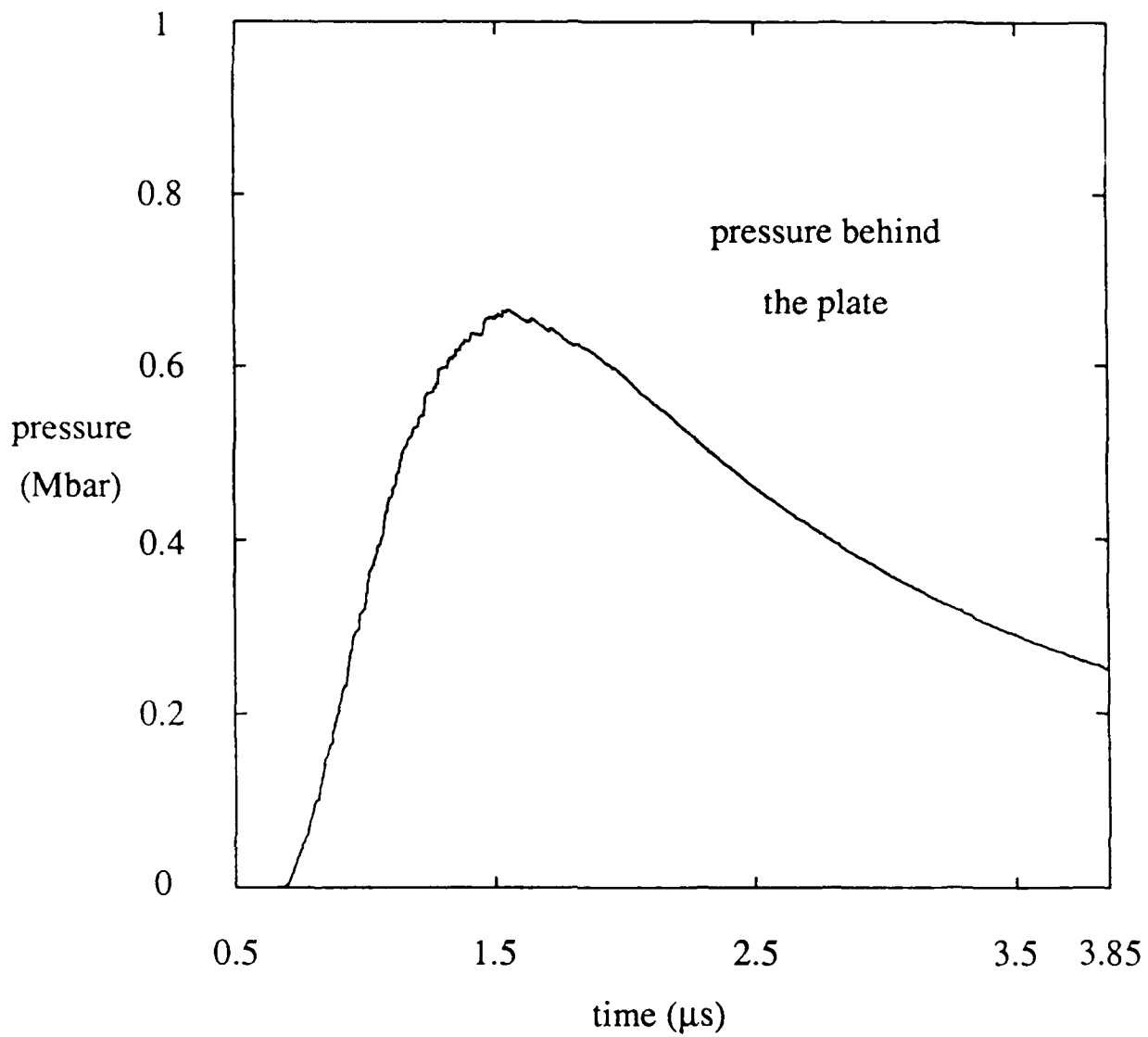


Figure 8. Pressure behind the plate. The pressure behind the tungsten plate is plotted as a function of time for the computation described in the caption for Fig. 6.

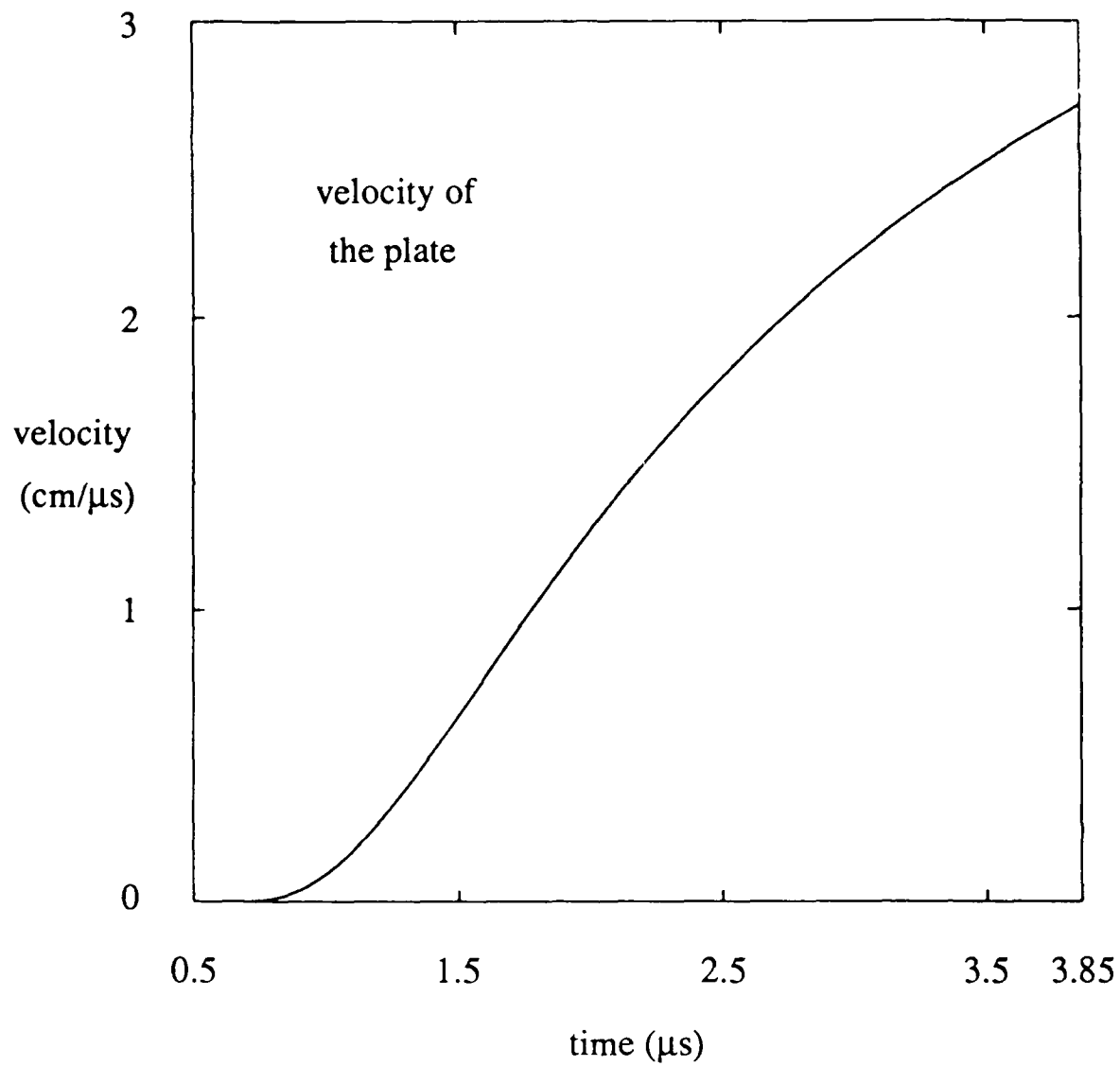


Figure 9. Velocity of the plate. The velocity of the tungsten plate is plotted as a function of time for the computation described in the caption for Fig. 6.

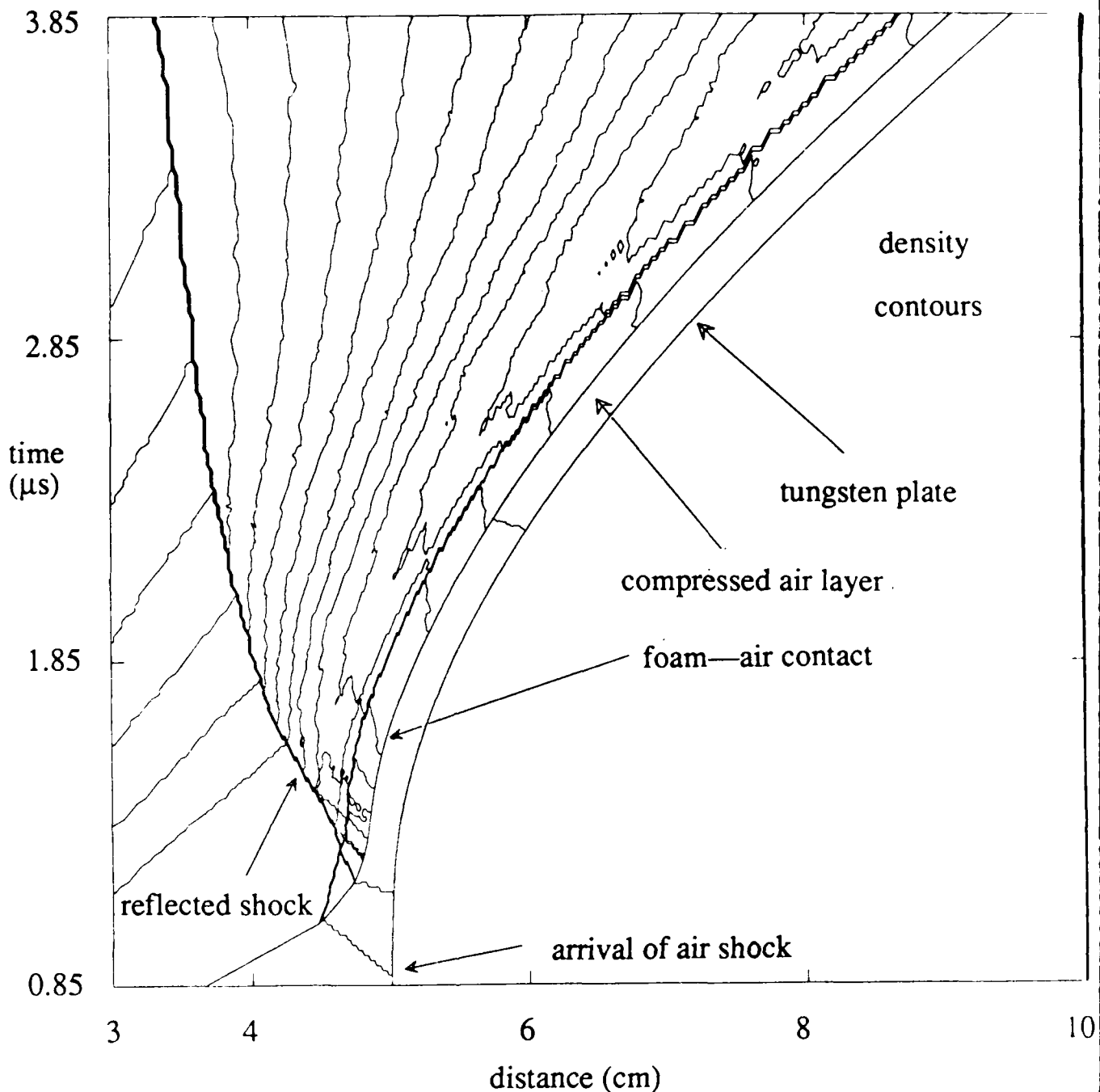


Figure 10. Density contours for shockless acceleration using an air-filled cavity. The foam is shocked as in the computation described in Fig. 6. At time $t = 0$ the shock reaches the end of the foam at $x = 0$, whereupon the foam expands into the cavity and compresses the air, thereby accelerating the tungsten plate. The air is initially at standard conditions, and the tungsten plate has an areal mass density of 0.5 g/cm^2 . A weak shock is transmitted to the air; its arrival at the plate is marked by a shock reflected from the plate. The contact discontinuity between the foam and the air interacts with waves reflected from the plate, which strengthen into a reflected shock that overtakes the expansion wave in the foam. A layer of compressed air moving with the plate separates the foam from the plate. The velocity of the plate at the $t = 3.85 \text{ } \mu\text{s}$ is $2.69 \text{ cm}/\mu\text{s}$. In this computation the foam—air contact and the tungsten plate are tracked, with the plate modeled as a movable wall. A 3:1 mesh refinement is used for $4 < x < 6 \text{ cm}$, as in Fig. 6.

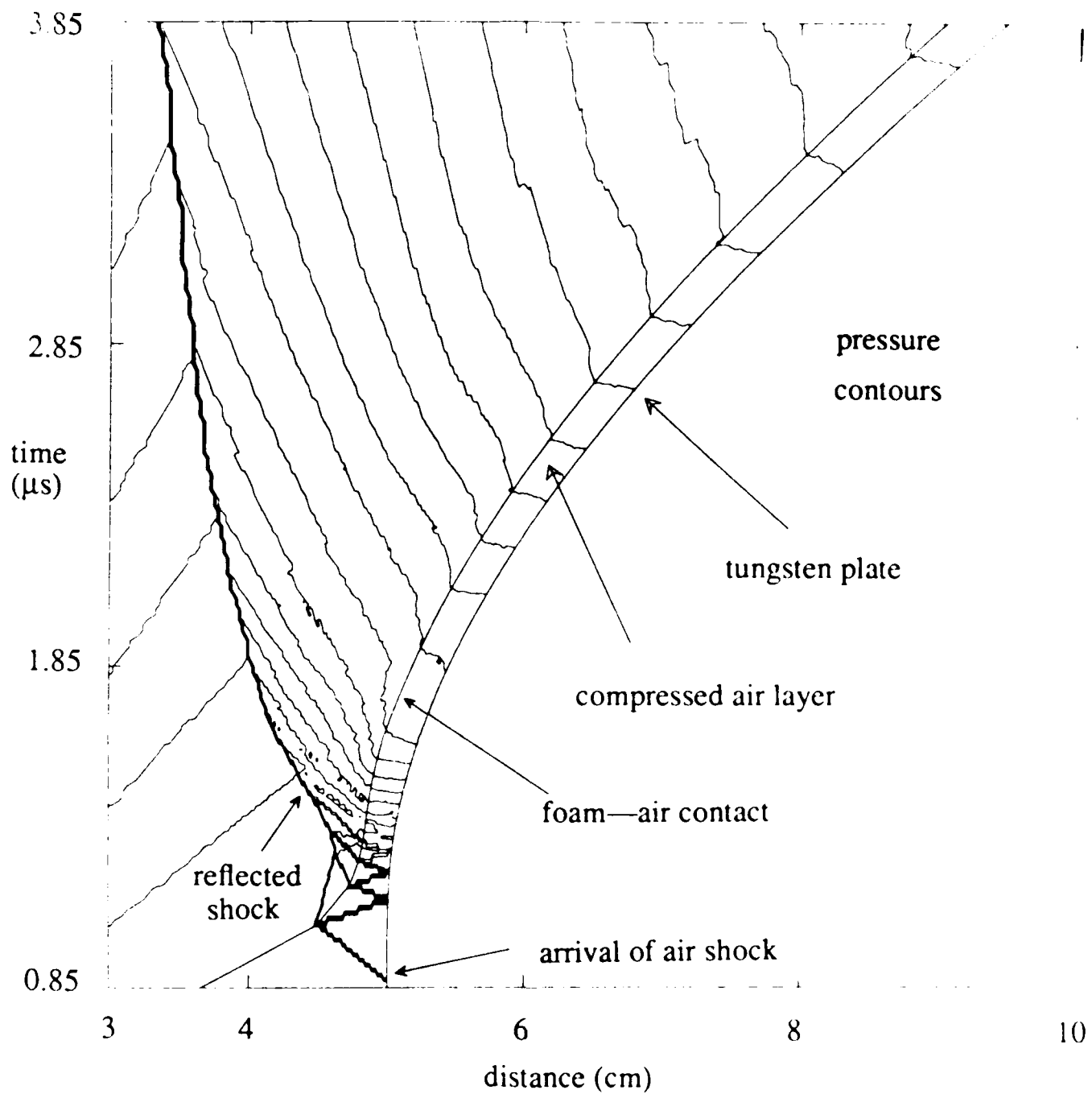


Figure 11. Pressure contours for shockless acceleration using an air-filled cavity. The space-time contours of pressure are shown for the computation described in the caption for Fig. 10. The succession of shock waves reflecting between the foam-air contact discontinuity and the tungsten plate can clearly be seen by comparing this figure with Fig. 10. Some waves, such as the first air shock that reflects from the foam-air contact, are visible in this figure but not in Fig. 10, whereas the secondary contact discontinuity in the foam is visible only in the density contour plot.

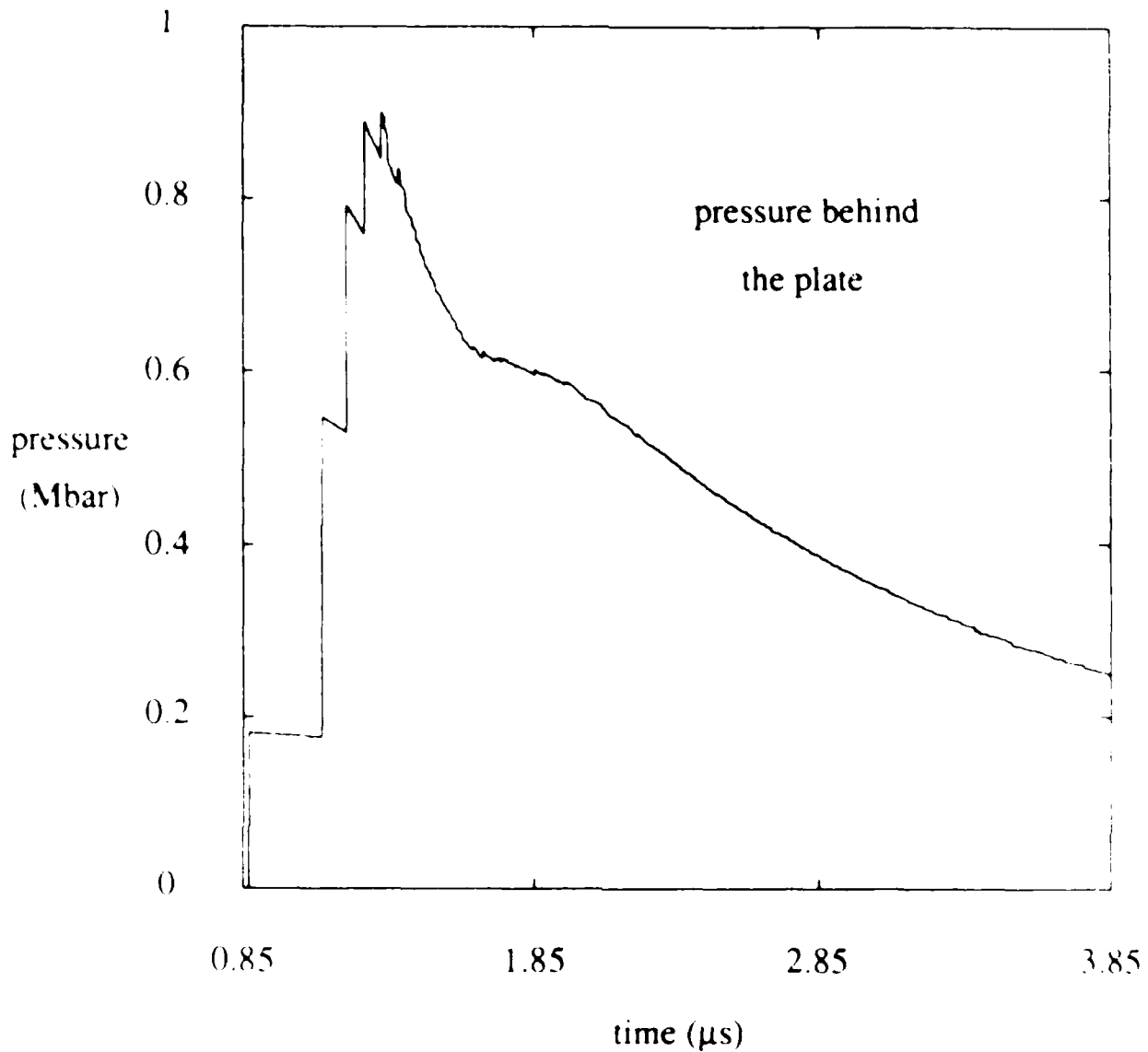


Figure 12. Pressure behind the plate. The pressure behind the tungsten plate is plotted as a function of time for the computation described in the caption for Fig. 10. The pressure jump at $t = 0.87$ is caused by the air shock hitting the plate, and the jumps that follow correspond to the succession of shock waves that reflect from the plate, as seen in Fig. 11. The hump at $t = 1.7$ corresponds to the arrival at the plate of signals from the right edge of the expansion wave in the foam; this is also seen in Fig. 11.

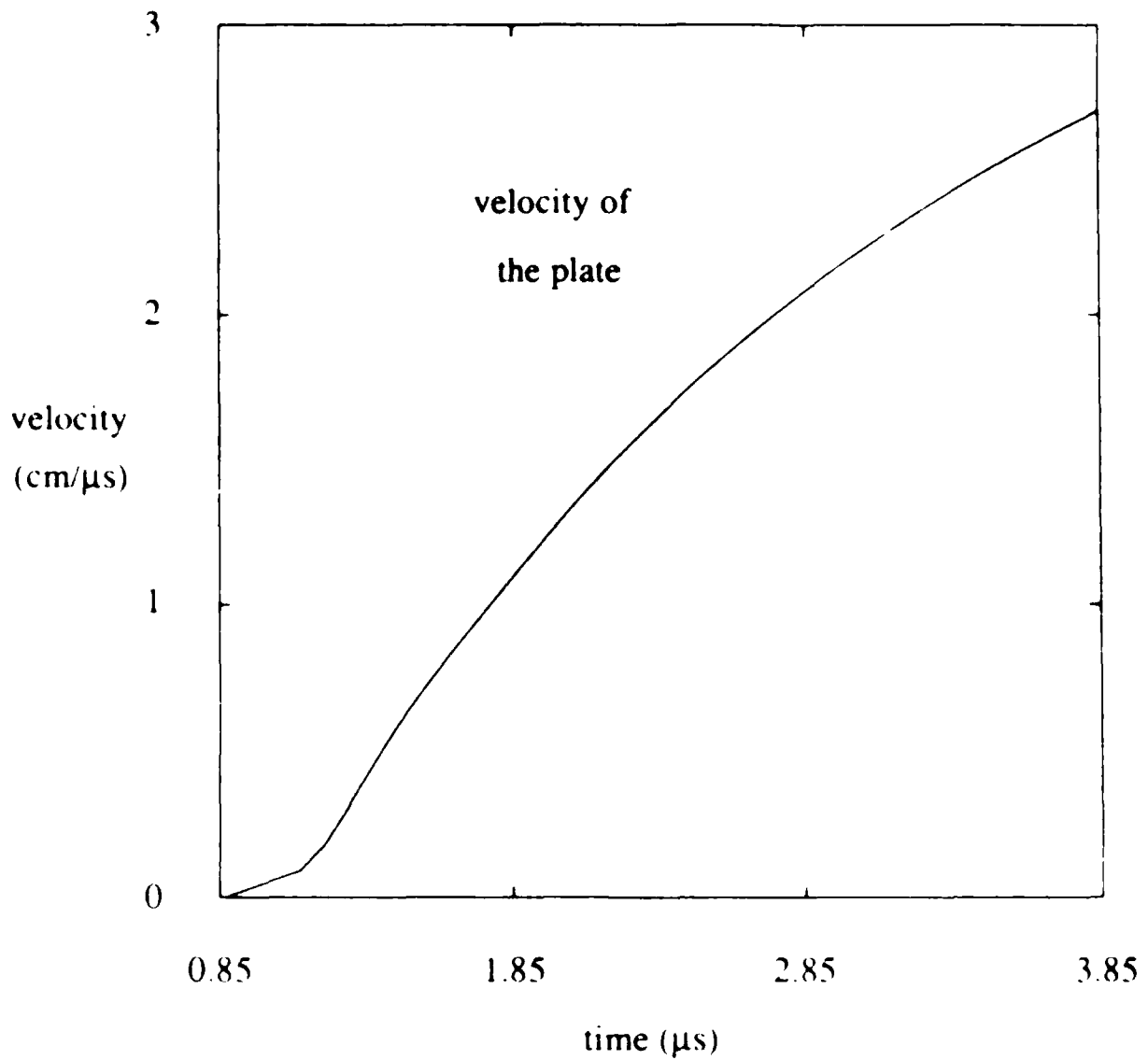


Figure 13. Velocity of the plate. The velocity of the tungsten plate is plotted as a function of time for the computation described in the caption for Fig. 10.

and 11. Some waves, such as the first air shock that reflects from the foam-air contact, are visible in pressure contours plot but not in the density contours plot, whereas the secondary contact discontinuity in the foam is visible only in the density contour plot.

The pressure behind the tungsten plate is plotted as a function of time in Fig. 12. The smooth rise in pressure seen in Fig. 8 has now become jagged during the early stages of the flow development, and the peak pressure is higher. The pressure jump at $t = 0.87$ is caused by the air shock hitting the plate, and the jumps that follow correspond to the succession of shock waves that reflect from the plate, as seen in Fig. 11. The hump at $t \approx 1.7$ corresponds to the arrival at the plate of signals from the right edge of the expansion wave in the foam; this is also seen in Fig. 11. Fig. 13 shows the velocity of the tungsten plate, plotted as a function of time. The kinks in this plot correspond to the discontinuities in Fig. 12. The velocity of the plate at $t = 3.85 \mu\text{s}$ is again $2.69 \text{ cm}/\mu\text{s}$.

Although the short-time development of the flow changes markedly when the cavity pressure is raised to as small a pressure as 10^{-6} Mbar, the long-time behavior of the flow and the accelerating plate is little affected. This is evident in the contour plots and the plots of the velocity of and pressure behind the plate. In fact, at late times the velocity and pressure for the air-filled cavity agree quantitatively with these quantities when the cavity is evacuated.

The reverberating shock waves that are present in the flow when the cavity has not been evacuated may cause damage to the accelerating plate, for instance through shock heating. To ascertain the effect that these air shocks have on the plate, the experiment with the air-filled cavity was simulated, during the early stages of the interaction, with the tungsten plate modeled as a thin (0.025 cm) layer of fluid. In this computation the equation of state of the tungsten is a stiffened gas, with $\gamma = 3.14$ and $p_{\infty} = 1.0 \text{ Mbar}$. The two sides of the plate are tracked, as is the foam-air contact discontinuity. A 10:1 mesh refinement is used for $4.95 < x < 5.25 \text{ cm}$, with a total of 300 mesh cells. With this mesh refinement there are approximately 10 mesh cells inside of the plate.

The results are shown in Figs. 14-18. Fig. 14 shows the space-time contours of pressure, in which the shocks that form inside the plate are evident. An expanded view of the pressure contours in the vicinity of the accelerating plate is shown in Fig. 15. The detailed internal structure of the flow inside the plate is evident in this plot. The corresponding plot of the pressure behind the plate, plotted as a function of time, is shown in Fig. 16. The pressure jump at $t = 0.87$ is caused by the air shock hitting the plate, and the jumps that follow correspond to the succession of shock waves that reflect from the plate, as seen in Figs. 14 and 15.

The relative velocity of the two sides of the plate is plotted as a function of time in Fig. 17. A positive relative velocity indicates expansion of the plate. The jumps in the expansion velocity correspond to waves in the air arriving at the plate and to waves in the plate reflecting from the ends of the plate, as seen in Fig. 15. Shock waves in the air that strike the back end of the plate transmit a shock wave into the plate and cause the relative velocity to drop. The transmitted shock reflects from the front end of the plate as a rarefaction wave and causes the relative velocity to rise. This simple ringing of the plate continues until interactions between waves creates broad rarefaction waves that complicate the flow.

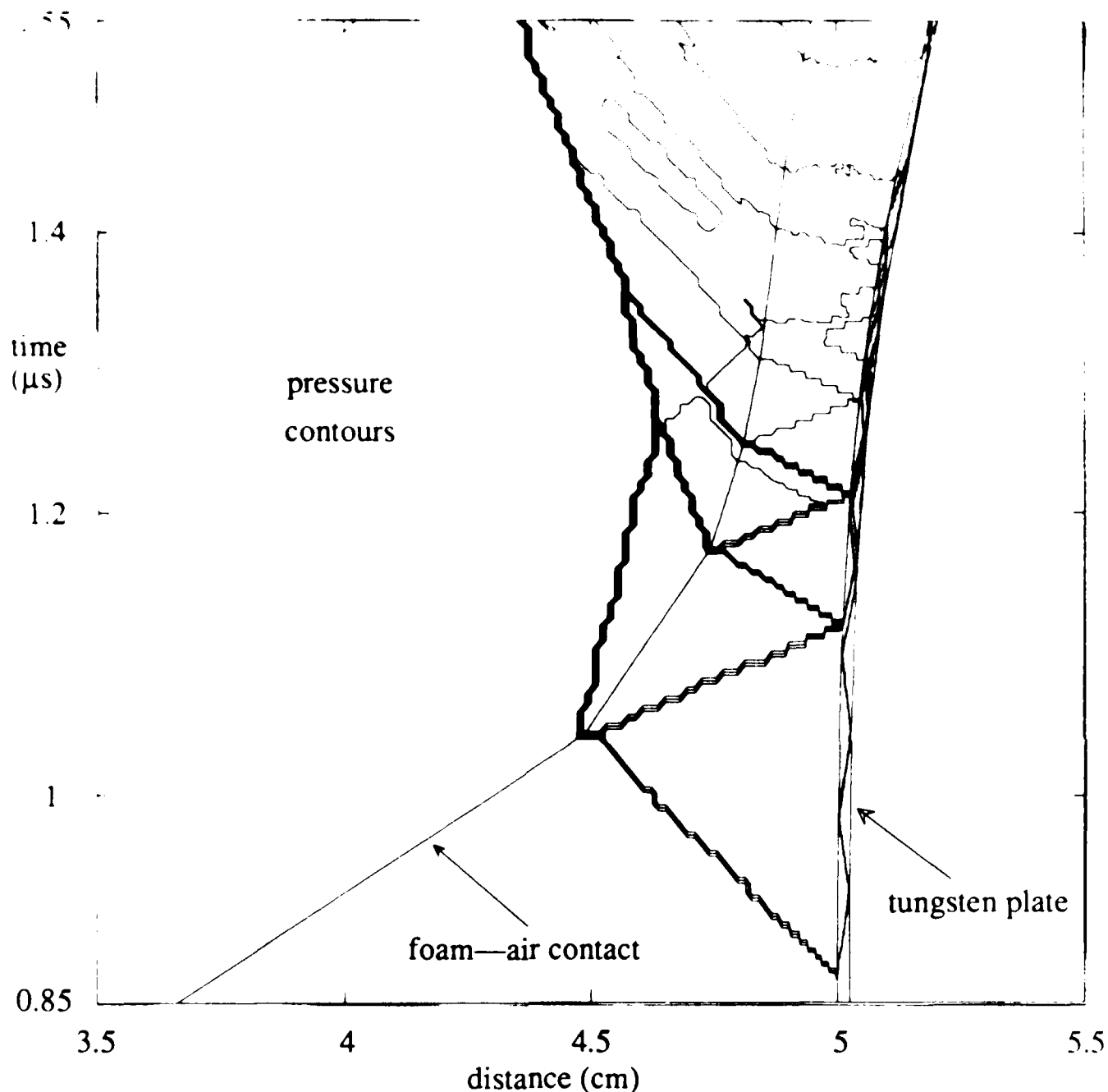


Figure 14. Pressure contours for shockless acceleration using an air-filled cavity. The space-time contours of pressure are shown for the early-time development in the computation described in the caption for Fig. 10. In this computation the tungsten plate is modeled as a stiffened gas. The two sides of the plate are tracked, as is the foam—air contact discontinuity. A 10:1 mesh refinement is used for $4.95 < x < 5.45$ cm, with a total of 300 mesh cells. With this mesh refinement there are approximately 10 mesh cells inside of the plate. The combination of mesh refinement, front tracking, and the random choice method is crucial to resolving the shock waves that can be seen propagating inside the plate.

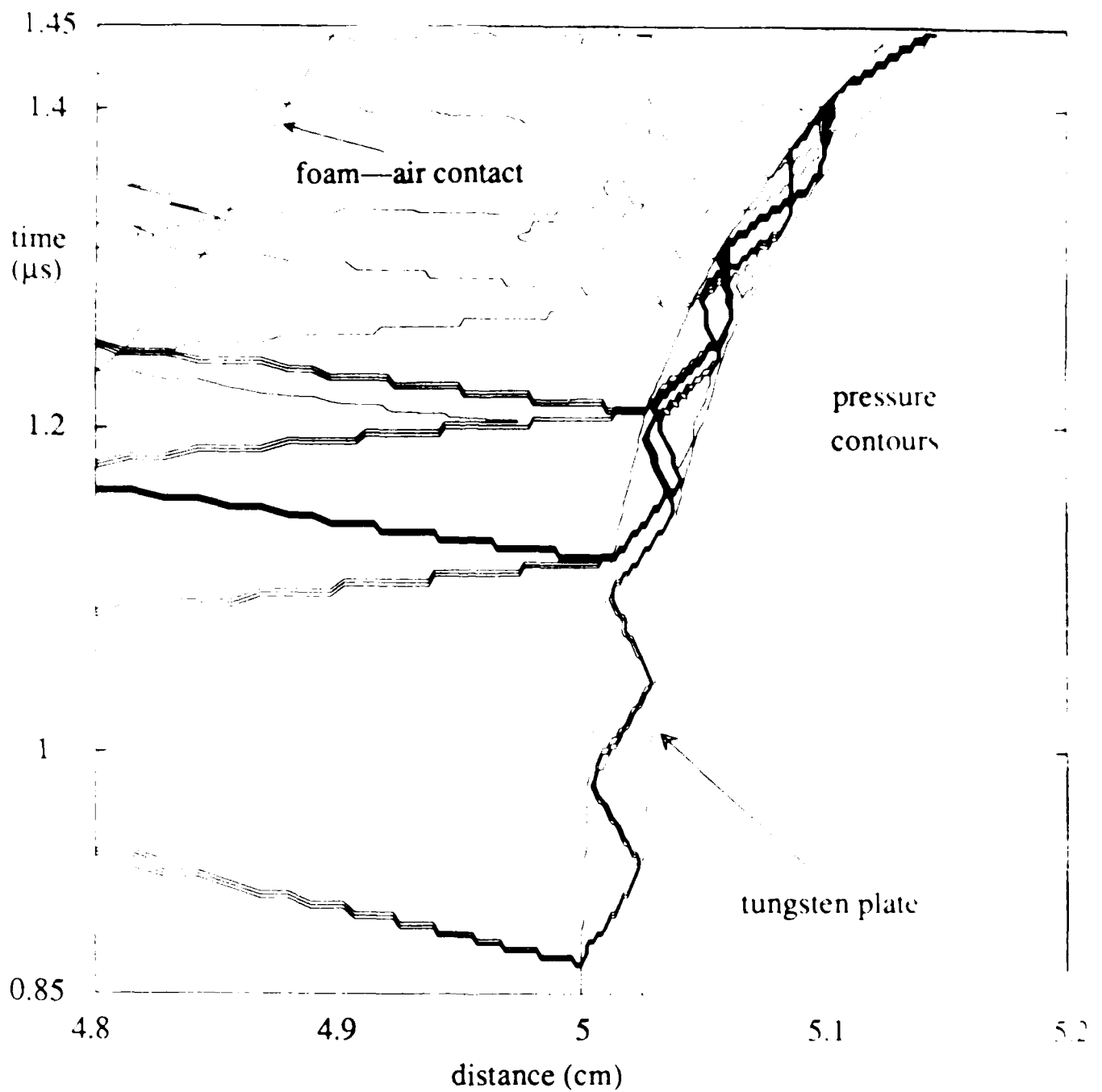


Figure 15. Expanded view of the plate. The pressure contours for the computation described in the caption for Fig. 14 are shown in the vicinity of the accelerating plate. The detailed internal structure of the flow inside the plate is evident in this plot.

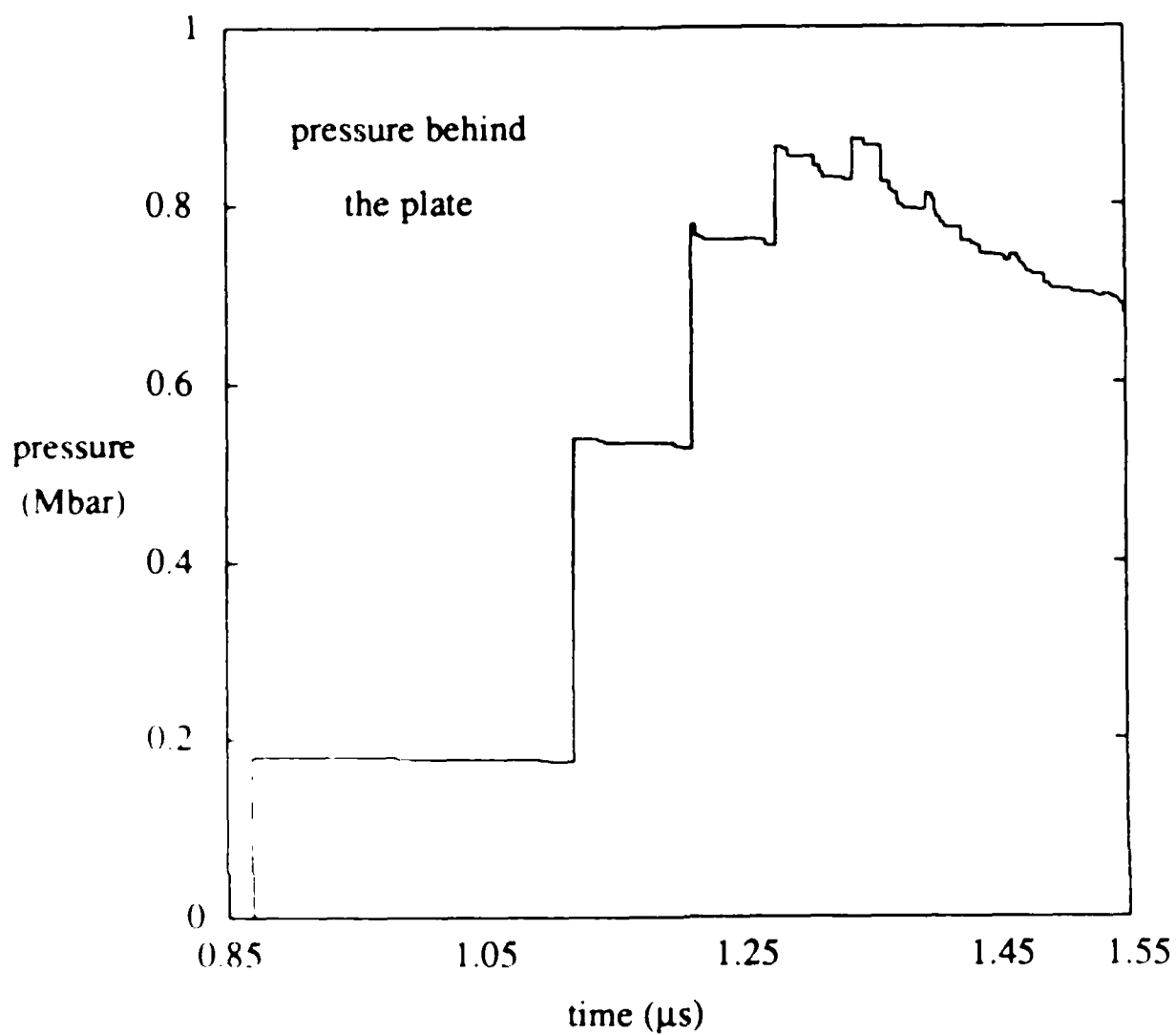


Figure 16. Pressure behind the plate. The pressure behind the tungsten plate is plotted as a function of time for the computation described in the caption for Fig. 14. The pressure jump at $t = 0.87$ is caused by the air shock hitting the plate, and the jumps that follow correspond to the succession of shock waves that reflect from the plate, as seen in Figs. 14 and 15.

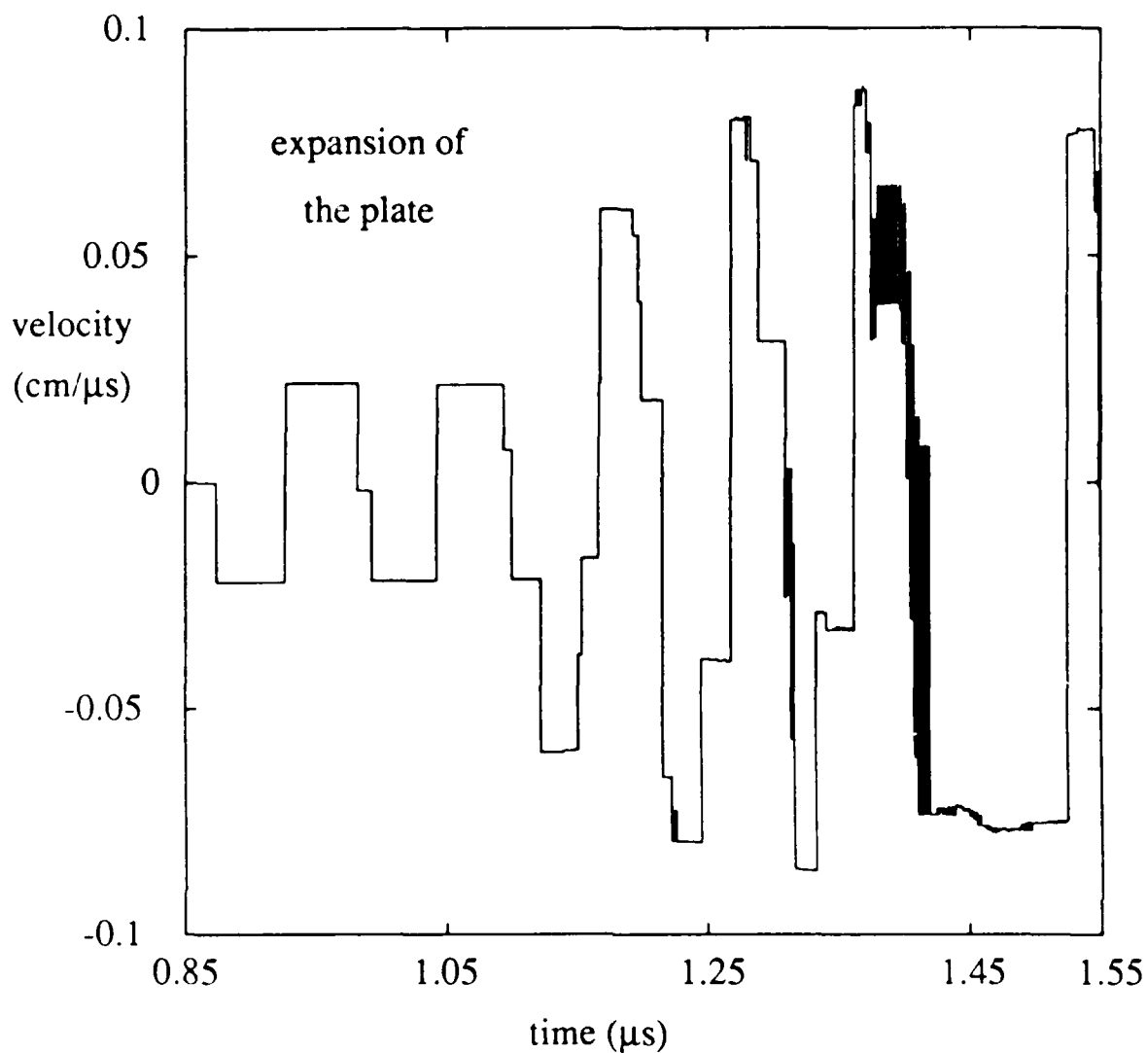


Figure 17. Expansion of the plate. The relative velocity of the two sides of the plate is plotted as a function of time for the computation described in the caption for Fig. 14. A positive relative velocity indicates expansion of the plate. The jumps in the expansion velocity correspond to waves in the air arriving at the plate and to waves in the plate reflecting from the ends of the plate, as seen in Fig. 15.

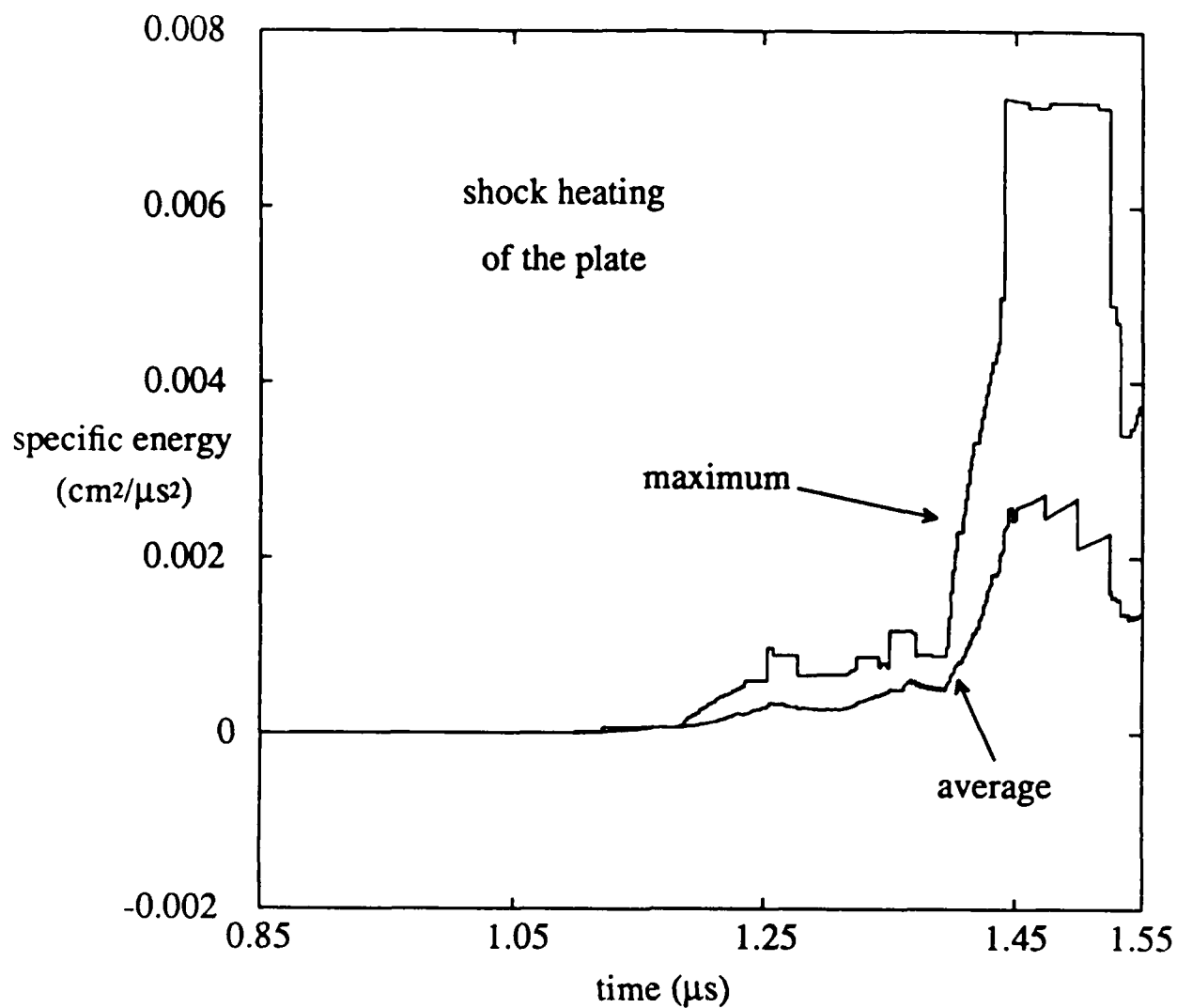


Figure 18. Shock heating inside the tungsten plate. An approximation ΔQ to the heat deposition inside the plate is shown. The maximum and the spatial average of ΔQ across the plate is plotted as a function of time. For comparison, the latent heat of fusion of tungsten at standard conditions is $0.0019 \text{ cm}^2/\mu\text{s}^2$.

Although the ringing of the plate is rather violent, the rarefaction waves never combine to put the material in tension, as they do in a spall experiment. (This is confirmed by plotting the minimum pressure in the plate as a function of time.) Within the confines of this simplistic model for the equation of state, therefore, it is expected that the plate will not spall when it is accelerated in the manner being investigated.

As another diagnostic measure for possible structural damage to the plate, the heat deposition in the plate due to shock waves should be determined. This heat deposition is to be compared to the heat of melting of tungsten to determine whether the plate melts. Since the plate is being accelerated by a light fluid, it is subject to Rayleigh-Taylor instability. Were the plate to melt, its material strength might not sufficiently dampen the growth of these instabilities, and it could be destroyed.

The stiffened gas equation of state is not complete, in that the temperature and entropy is not determined. In place of using a complete equation of state, an approximation to the heat deposition in the plate is determined by comparing the computed specific energy in the plate with the specific energy that would be in the plate if the plate had been isentropically compressed. Let

$$E = \frac{1}{\gamma - 1} \frac{p + p_{\infty} + (\gamma - 1)p_{\infty}}{\rho}$$

be the specific energy in a given computational mesh cell inside the plate, and let

$$E_{S_0} = \frac{1}{\gamma - 1} \frac{(\rho/\rho_0)^{\gamma}(p_0 + p_{\infty}) + (\gamma - 1)p_{\infty}}{\rho}$$

be the corresponding specific energy of the cell were it to have been compressed isentropically from its initial state with density ρ_0 and pressure p_0 . (See Eq. 2.1.) We then define

$$\Delta Q = E - E_{S_0} \approx T \Delta S$$

to be an effective heat deposition in the cell. The maximum of this quantity over the plate and its spatial average is plotted as functions of time in Fig. 18. Since the latent heat of fusion of tungsten at standard conditions is $0.0019 \text{ cm}^2/\mu\text{s}^2$, which is of the same order of magnitude as ΔQ , no definitive conclusion can be drawn from the calculation, although it suggests that the plate might melt.

Conclusions

These computations demonstrate the ability of our numerical method to resolve the highly complicated flows that arise in McCall's method for accelerating thin plates. The combination of mesh refinement, front tracking, and the random choice method is crucial to resolving shock waves propagating inside the plate.

The short-time asymptotic solution and the computational results confirm that shock waves do not form inside a sufficiently thin plate, provided that the cavity between the propellant foam and the plate has been evacuated. The computations do show, however, that it is critical to have a good vacuum in the cavity: pressures of only 10^{-6} on the scale of pressures being considered give rise to significant shock waves in the plate. These shock waves cause violent ringing of the plate, but they never put the plate into tension; thus according to the model used, the plate does not spall. The shock waves also heat the plate, and a simple estimate of this effect indicates that the plate might melt. This melting would make the plate more susceptible to Rayleigh-Taylor instability.

In combination with a better model of the structural properties of the tungsten plate, the results of these hydrodynamic calculations can be used to more conclusively determine the feasibility of McCall's method for shockless acceleration of thin plates.

Acknowledgements

The author is grateful to R. Menikoff for contributing many ideas in the physical interpretation of the numerical results. He also thanks J. Glimm and D. Sharp for their support and encouragement.

References

1. *LASL Shock Hugoniot Data*, ed. S. Marsh, University of California Press, Berkeley, 1980.
2. *T-4 Handbook of Material Properties Data Bases, Vol. 1c: Equations of State*, ed. K. Holian, Los Alamos National Laboratory, 1984.
3. A. Chorin, "Random Choice Solutions of Hyperbolic Systems," *J. Comp. Phys.* **22** (1976), pp. 517-533.
4. J. Glimm, "Solutions in the Large for Nonlinear Hyperbolic Systems of Equations," *Comm. Pure Appl. Math.* **XVIII** (1965), pp. 697-715.
5. J. Glimm, D. Marchesin, and O. McBryan, "Subgrid Resolution of Fluid Discontinuities II," *J. Comp. Phys.* **37** (1980), pp. 336-354.
6. S. Godunov, "A Difference Method for Numerical Calculation of Discontinuous Solutions of the Equations of Hydrodynamics," *Mat. Sb.* **47** (1959), pp. 271-306.
7. H. Greenspan and D. Butler, "On the Expansion of a Gas into a Vacuum," *J. Fluid Mech.* **13** (1962), pp. 101-119.
8. F. Harlow and A. Amsden, "Fluid Dynamics," LANL Monograph LA-4700, 1971.
9. A. Love and F. Pidduck, "Lagrange's Ballistic Problem," *Trans. Royal Soc. London* **222** (1922), pp. 167-226.
10. G. McCall, "A Method for Producing Shockless Acceleration of Masses to Hyper-velocities Using High Explosives," Report LJI-TM-84-106, La Jolla Institute, May, 1984.

A181015

REPORT DOCUMENTATION PAGE		READ INSTRUCTIONS BEFORE COMPLETING FORM
1. REPORT NUMBER 2968	2. GOVT ACCESSION NO.	3. RECIPIENT'S CATALOG NUMBER
4. TITLE (and Subtitle) MODELING OF SHOCKLESS ACCELERATION OF THIN PLATES USING A TRACKED RANDOM CHOICE METHOD		5. TYPE OF REPORT & PERIOD COVERED Summary Report - no specific reporting period
		6. PERFORMING ORG. REPORT NUMBER
7. AUTHOR(s) Bradley J. Plohr		8. CONTRACT OR GRANT NUMBER(s) DAAG29-80-C-0041 DMS-8601766
9. PERFORMING ORGANIZATION NAME AND ADDRESS Mathematics Research Center, University of 610 Walnut Street Madison, Wisconsin 53705		10. PROGRAM ELEMENT, PROJECT, TASK AREA & WORK UNIT NUMBERS Work Unit Number 2 - Physical Mathematics
11. CONTROLLING OFFICE NAME AND ADDRESS See Item 18 below.		12. REPORT DATE February 1987
		13. NUMBER OF PAGES 39
14. MONITORING AGENCY NAME & ADDRESS (if different from Controlling Office)		15. SECURITY CLASS. (of this report) UNCLASSIFIED
		15a. DECLASSIFICATION/DOWNGRADING SCHEDULE
16. DISTRIBUTION STATEMENT (of this Report) Approved for public release; distribution unlimited.		
17. DISTRIBUTION STATEMENT (of the abstract entered in Block 20, if different from Report)		
18. SUPPLEMENTARY NOTES U. S. Army Research Office P. O. Box 12211 Research Triangle Park North Carolina 27709 National Science Foundation Washington, DC 20550		
19. KEY WORDS (Continue on reverse side if necessary and identify by block number) shockless acceleration Riemann problem random choice front tracking		
20. ABSTRACT (Continue on reverse side if necessary and identify by block number) A method for accelerating thin metallic plates to hypervelocities has been proposed by G. McCall. ¹⁰ In this method a shock in a propellant generates a strong expansion wave that smoothly accelerates the plate. We have studied the hydrodynamics of this process in one dimension, both analytically and computationally. The metal was modeled as a stiffened gas, and the corresponding Riemann problem was solved. The asymptotic behavior of the solution was determined analytically. The one-dimensional random choice		

20. ABSTRACT - cont'd.

method, modified so that material boundaries are tracked and the spatial mesh is refined locally, was used to compute the flow; comparison with the asymptotic solution demonstrated its accuracy. With this method, shocks that form within the accelerating plate were accurately resolved, so that possible structural damage to the plate could be evaluated.

END

7-87

DTIC